BBA - Bioenergetics 1862 (2021) 148367

Contents lists available at ScienceDirect

BBA - Bioenergetics

journal homepage: www.elsevier.com/locate/bbabio

Soluble adenylyl cyclase regulates the cytosolic NADH/NAD$^+$ redox state and the bioenergetic switch between glycolysis and oxidative phosphorylation

Jung-Chin Chang [a,b,*], Simei Go [a,b], Eduardo H. Gilglioni [a,c], Suzanne Duijst [a], Daan M. Panneman [d], Richard J. Rodenburg [d,e], Hang Lam Li [a,f], Hsu-Li Huang [a,f], Lonny R. Levin [g], Jochen Buck [g], Arthur J. Verhoeven [a], Ronald P.J. Oude Elferink [a,b]

[a] Tytgat Institute for Liver and Intestinal Research, Amsterdam UMC, University of Amsterdam, Amsterdam, the Netherlands
[b] Amsterdam Gastroenterology Endocrinology Metabolism (AGEM) Research Institute, Amsterdam UMC, University of Amsterdam, Amsterdam, the Netherlands
[c] University of Maringá, Department of Biochemistry, Paraná, Brazil
[d] Radboud Center for Mitochondrial Medicine, Department of Pediatrics, Amalia Children's Hospital, Radboudumc, Nijmegen, the Netherlands
[e] Translational Metabolic Laboratory, Department of Laboratory Medicine, Radboudumc, Nijmegen, the Netherlands
[f] School of Medicine, National Taiwan University, Taipei, Taiwan
[g] Department of Pharmacology, Weill Cornell Medical College, New York, USA

ARTICLE INFO

Keywords:
Soluble adenylyl cyclase
Exchange protein directly activated by cAMP (Epac)
Protein kinase A
Glycolysis
Oxidative phosphorylation
NADH/NAD$^+$ redox state

ABSTRACT

The evolutionarily conserved soluble adenylyl cyclase (sAC, *ADCY10*) mediates cAMP signaling exclusively in intracellular compartments. Because sAC activity is sensitive to local concentrations of ATP, bicarbonate, and free Ca^{2+}, sAC is potentially an important metabolic sensor. Nonetheless, little is known about how sAC regulates energy metabolism in intact cells. In this study, we demonstrated that both pharmacological and genetic suppression of sAC resulted in increased lactate secretion and decreased pyruvate secretion in multiple cell lines and primary cultures of mouse hepatocytes and cholangiocytes. The increased extracellular lactate-to-pyruvate ratio upon sAC suppression reflected an increased cytosolic free [NADH]/[NAD$^+$] ratio, which was corroborated by using the NADH/NAD$^+$ redox biosensor Peredox-mCherry. Mechanistic studies in permeabilized HepG2 cells showed that sAC inhibition specifically suppressed complex I of the mitochondrial respiratory chain. A survey of cAMP effectors revealed that only selective inhibition of exchange protein activated by cAMP 1 (Epac1), but not protein kinase A (PKA) or Epac2, suppressed complex I-dependent respiration and significantly increased the cytosolic NADH/NAD$^+$ redox state. Analysis of the ATP production rate and the adenylate energy charge showed that inhibiting sAC reciprocally affects ATP production by glycolysis and oxidative phosphorylation while maintaining cellular energy homeostasis. In conclusion, our study shows that, via the regulation of complex I-dependent mitochondrial respiration, sAC-Epac1 signaling regulates the cytosolic NADH/NAD$^+$ redox state, and coordinates oxidative phosphorylation and glycolysis to maintain cellular energy homeostasis. As such, sAC is effectively a bioenergetic switch between aerobic glycolysis and oxidative phosphorylation at the post-translational level.

1. Introduction

The 3′,5′-cyclic adenosine monophosphate (cAMP) generated by transmembrane adenylyl cyclases (tmAC, *ADCY1–9*) is a versatile second messenger of G-protein-coupled receptors (GPCRs) signaling, originally discovered by Earl Sutherland to mediate glucagon and epinephrine-induced glycogenolysis [1]. Apart from regulating glycogen metabolism, glucagon and epinephrine also regulate glycolysis and lipolysis via tmAC-generated cAMP and protein kinase A (PKA). Later, a new type of mammalian soluble adenylyl cyclase (sAC, *ADCY10*) was discovered, which is evolutionarily more ancient than tmACs and is not localized at the plasma membrane [2,3]. The intracellularly localized sAC and the plasma-membrane-localized tmACs share common cAMP effectors, such as PKA and "exchange factor directly activated by

* Corresponding author at: Tytgat Institute for Liver and Intestinal Research, Amsterdam UMC, University of Amsterdam, Amsterdam, the Netherlands.
E-mail address: j.chang@amsterdamumc.nl (J.-C. Chang).

https://doi.org/10.1016/j.bbabio.2020.148367
Received 13 May 2020; Received in revised form 11 December 2020; Accepted 19 December 2020
Available online 5 January 2021

cAMP" (Epac1 and Epac2). However, sAC is not regulated by G-proteins and does not respond to forskolin, a general tmAC activator [3]. Instead, in cells, sAC activity reflects physiological levels of cellular bicarbonate and is synergistically stimulated by Ca^{2+} [2,4,5]. In contrast to the well-established role of tmAC-dependent cAMP signaling in metabolic regulation, our knowledge about the regulation of cellular metabolism by sAC-generated cAMP is limited.

GPCR-dependent cAMP signaling appeared first in metazoa to serve hormone-mediated intercellular communication while sAC-like enzymes first appeared in unicellular organisms as a CO_2/HCO_3^- sensor [2,3]. As bicarbonate and CO_2 are primary products during bioenergetic processes (e.g. the Krebs cycle), sAC is proposed to be a putative metabolic sensor [6]. This concept is supported by several biochemical characteristics of the enzyme. Firstly, sAC homologs in multicellular as well as in unicellular organisms can be activated by bicarbonate (reviewed in [7]). Secondly, compared to tmACs, sAC has a much higher K_m for its substrate ATP (ranging from 1 to 10 mM), which allows ATP sensing [4,8,9]. Thirdly, albeit often at a low level, sAC is expressed in almost all tissues examined [10,11]. Moreover, sAC activity is synergistically stimulated by Ca^{2+}, another versatile and universal second messenger [9,10], allowing sAC to integrate cellular metabolism with signaling transduction. Supporting this reasoning, sAC was demonstrated to regulate oxidative phosphorylation by sensing CO_2 production from the TCA cycle [12] and/or free Ca^{2+} concentrations in the mitochondrial matrix [13], ATP-dependent insulin secretion in the pancreas [8], and TNF-induced respiratory burst in human neutrophils [14]. Due to accumulating evidence that sAC-generated cAMP regulates mitochondrial oxidative phosphorylation, bioenergetic regulation by sAC has often been studied using isolated mitochondria [12,15,16]. Although mouse embryonic fibroblasts (MEFs) prepared from sAC C1KO mice (generated by knock-out of exon 2–4 of the first catalytic domain) were shown to have increased proton secretion and reduced oxygen consumption compared to wild-type MEF [17], the acute bioenergetic regulation by sAC in whole cells is unknown. In addition, a somatic sAC isoform transcribed from a downstream alternative start site in intron 5 was reported to be present in sAC C1KO mice [18]. Therefore, the role of sAC in the acute bioenergetic regulation at the whole cell level remains to be firmly established and the general presence of sAC-mediated bioenergetic regulation has yet to be explored. In this study, we demonstrate by a combined pharmacological and genetic approach that sAC regulates the cytosolic $NADH/NAD^+$ redox state and coordinate glycolysis and oxidative phosphorylation for cellular energy homeostasis in different cell lines and primary cells. Mechanistic studies revealed that sAC exerts its bioenergetic regulation by controlling complex I activity of the mitochondrial electron transport chain. Furthermore, we identify Epac1 as a direct downstream cAMP effector of sAC-mediated bioenergetic regulation.

2. Materials and methods

2.1. Materials

Unless otherwise indicated, materials were purchased from Sigma-Aldrich. pLKO.1-puro was a gift from Dr. David Root (Addgene plasmid # 10878) [19]. pCW-Cas9 was a gift from Dr. Eric Lander & Dr. David Sabatini (Addgene plasmid # 50661) [20]. pcDNA3.1-Peredox-mCherry was a gift from Dr. Gary Yellen (Addgene plasmid # 32383) [21]. pcRDNA3.1-hygro-cyto-iNap1 and pcRDNA3.1-hygro-cyto-iNapc were kind gifts from Dr. Yi Yang [22].

2.2. Methods

2.2.1. Cell line cultures

The immortalized human cholangiocytes H69 are a kind gift from Douglas Jefferson [23] and were cultured in DMEM/F-12 (3:1) with hormonal supplements as described [24]. HepG2, Caco-2, B16F10, and Raw264.7 were cultured in DMEM (Invitrogen) with 2 g/L glucose, 1.8 g/L $NaHCO_3$, 20 mM HEPES-NaOH pH 7.4 and 10% fetal bovine serum.

For extracellular flux analysis by the Seahorse XFe96 Analyzer, cells were cultured in 50 μL culture medium. To avoid culture artifacts caused by medium evaporation, culture plates were placed in a custom-made humidity chamber inside a 5% CO_2 incubator. For all experiments, the incubation medium of cells was refreshed the day before experiments.

2.2.2. Isolation and culture of primary mouse hepatocytes, primary mouse cholangiocytes, and primary human cholangiocytes

Wild-type C57BL/6 J mice (obtained from Envigo) were maintained under the standard pathogen-free condition. Animal experiments were approved by the institutional animal experiment committee. Primary mouse hepatocytes were isolated from wild-type C57BL/6 J mice after overnight ad libitum feeding by a two-step collagenase perfusion method through the portal vein [25]. Primary mouse hepatocytes were cultured in collagen-coated plates in a 5% CO_2, 37 °C incubator.

Primary mouse cholangiocytes were isolated from wild-type C57BL/6 J and cultured as previously described [24]. Primary human cholangiocytes isolated from normal liver tissues are a kind gift from Dr. Jesus Banales and were cultured as previously described [26].

2.2.3. Construction of lentiviral vectors and lentiviral production

The cloning procedure and short hairpin oligo sequences used to construct tetracycline-inducible lentiviral vector for sAC knockdown and scramble control have been described previously [24]. Using pLKO.1-puro, the same procedure was followed to construct constitutively active lentiviral vectors for sAC knockdown and scramble control.

We generated stable cell lines expressing the inducible Peredox-mCherry $NADH/NAD^+$ redox sensor, iNap1 NADPH sensor, and iNapc (control for iNap1). Briefly, the puromycin resistance gene of pCW-Cas9-Puro was removed by *Hinc*II and *Xba*I. The blasticidin resistance gene (Bsd) was amplified by forward primer 5′-CAGTCGGCTCCCTCGTTGACCGAATCACCGACCTCTCTCCCCAGACGCGTATGGCCAAGCCTTTGTCTCA-3′ and reverse primer 5′-TTGTCCAGTCTAGACATTGGACCAGGGTTTTCTTCAACATCACCACAAGTGAGGAGAGAACCTCTACCTTCATGCATGCCCTCCCACACATAAC-3′. The purified PCR fragment was digested with *Hinc*II and Xbal and ligated with the open pCW-Cas9. The Cas9 insert was then removed by restriction enzymes *Nhe*I and BamHI. To create a multiple cloning site, the sense oligo (5′-CTAGCGTCGACACCGGTGAATTCGTTTAAACCCTGCAGGG-3′) and the antisense oligo (5′-GATCCCCTGCAGGGTTTAAACGAATTCACCGGTGTCGACG-3′) were annealed and ligated to the pCW backbone for pCW-MCS-BSD. The Peredox-mCherry insert was prepared by digesting pcDNA3.1-Peredox-mCherry with *Xba*I and *Pme*I. The inserts for NADPH biosensor iNap1 and sensor control iNapc were prepared by digesting pcRDNA3.1-hygro-cyto-iNap1 and pcRDNA3.1-hygro-cyto-iNapc with *Nhe*I and PmeI. The pCW-MCS-BSD vector was digested with NheI and PmeI and was ligated with the Peredox-mCherry insert, the iNap1 insert, and the iNapc insert for pCW-Peredox-mCherry-BSD, pCW-iNap1-BSD, and pCW-iNapc-BSD, respectively. Lentivirus was produced in HEK293T cells using the third-generation lentiviral packaging system. For the generation of stable cell lines, cells were transduced with lentivirus and selected with 2.5 μg/mL puromycin or 5 μg/mL Blasticidin according to the selection markers. In acute transduction experiments, the transduced cells were used without antibiotic selection.

2.2.4. Metabolomics study

Confluent HepG2 monolayers in 6-well plates were allowed to equilibrate in bicarbonate-free Hank's balanced salt solution (HBSS) with 5.5 mM glucose in ambient air at 37 °C for 1 h (please refer to Supplementary Table 1 for formulation). Cells were then treated with 50 μM LRE1 or vehicle control (0.1% DMSO) for 1 h. At the end of the incubation, medium was aspirated and metabolism was quenched by adding 0.5 mL −20 °C methanol. Subsequently, 0.5 mL ice-cold water

was added and cells were scraped and collected into a 2 mL Eppendorf tube. The homogenate was transferred to a 2 mL tube and incubated on ice for 10 min with occasional mixing. Then, 1 mL of chloroform was added, the homogenate was vortexed and centrifuged for 5 min at 20,000 ×*g* at 4 °C. The top layer was transferred to a new 1.5 mL tube and was dried in a vacuum centrifuge. Dried samples were dissolved in 100 μL methanol/water (*v*/v: 6/4). For analysis, we used a Thermo Scientific ultra-high-pressure liquid chromatography (UHPLC) system (Waltman, MA, USA) coupled to the Thermo Q Exactive (Plus) Orbitrap mass spectrometer (Waltman, MA, USA). The autosampler was kept at 10 °C during the run and 5 μL of sample was injected on the analytical column. The chromatographic separation was established using a SeQuant ZIC-cHILIC column (PEEK 100 × 2.1 mm, 3.0 μm particle size, Merck, Darmstadt, Germany) at 15 °C. The flow rate was 0.250 mL/min. The mobile phase was composed of solution A (acetonitrile/water (9:1) with 5 mM ammonium acetate, pH 6.8) and solution B (acetonitrile/water (1:9) with 5 mM ammonium acetate, pH 6.8). The UHPLC gradient program was as follows: 100% solution A at time 0–3 min, ramping to 20% solution A and 80% solution B during the 3–24 min interval, holding at 20% solution A and 80% solution B at 24–27 min, ramping to 100% solution A during the 27–28 min interval, and re-equilibration with 100% solution A at 28–35 min. The MS data were acquired in negative mode at full scan range at 140,000 resolution. Interpretation of the data was performed using the Xcalibur software (Thermo Scientific). Statistical analysis and visualization of the acquired data were performed using ggplot, ropls33, and mixOmics34 packages in the statistical programming language R (http://www.r-project.org). Missing values were excluded from statistical tests.

2.2.5. Sample preparation for enzymatic determination of glucose, L-lactate, and pyruvate

Cells were refreshed with culture medium 1 day prior to the experiment. On the day of the experiment, medium was changed to the experimental medium and cells were allowed to equilibrate in the experimental medium for 1 h. The experimental medium was DMEM without glutamine, with 5.5 mM glucose and 10% fetal bovine serum (Fig. 2) or 1% fetal bovine serum (Fig. S2). In all other experiments, the experimental medium was bicarbonate-free HBSS (see Table S1 for formulation) with 5.5 mM glucose. We did not observe any effect of amino acids on the acute regulation of cellular bioenergetics by sAC. At the start of the experiment, cells were exposed to media containing the indicated inhibitors and vehicle controls. At indicated time points, 50 μL spent medium was harvested and mixed with 75 μL ice-cold 5% (*w*/*v*) metaphosphoric acid (MPA) for deproteinization. After incubating for at least 1 h at 4 °C, the MPA-acidified samples were centrifuged at 20,000 ×*g* for 10 min. The supernatants were harvested for enzymatic determination of L-lactate, pyruvate, and glucose. For the determination of intracellular L-lactate and pyruvate, medium was aspirated. Cells cultured in 6-well plates were washed once with ice-cold PBS and lysed in 100 μL 3% ice-cold MPA. The acid homogenates were incubated at least 1 h at 4 °C and cleared by centrifuging at 20,000 ×*g* for 10 min at 4 °C. Lactate, pyruvate, and glucose are stable in 3% MPA at 4 °C and were assayed directly from the MPA extracts.

2.2.6. Enzymatic assay for glucose, L-lactate, and pyruvate

The enzymatic determinations of L-lactate, pyruvate and glucose were performed as previously described using a CLARIOstar microplate reader (BMG LABTECH) [25]. Briefly, glucose was assayed by a colorimetric assay with glucose oxidase (Sigma G-6641) according to Blake and McLean with modification for the microplate reader [27]. Pyruvate was assayed by a homovanillic acid-based fluorometric assay with pyruvate oxidase (Sigma P-4591) according to Zhu et al. with modifications [28]. L-Lactate was assayed with lactate dehydrogenase (Roche) according to Marbach and Weil with modification for the microplate reader [29]. Standards were prepared in 3% MPA and assayed simultaneously with the samples. Samples were diluted in 3% MPA as necessary.

2.2.7. Enzymatic assays for glucose-6-phosphate and 6-phosphogluconate

HepG2 cells were treated with 0.1% DMSO or 50 μM LRE1 for 15 min. After removing the medium, cells were washed with HBSS and deproteinized in 3% (*w*/*v*) $HClO_4$ (final concentration) on ice for 10 min. Deproteinized extracts were neutralized with 2.5 M K_2CO_3 and frozen at −80 °C until analysis. After thawing and removal of the $KClO_4$ precipitate, 50 μL of samples was mixed with 150 μL assay buffer (50 mM Tris-HCl, 8 mM $MgCl_2$, 4 mM EDTA-NaOH (pH 7.4) and 0.5 mg/mL $NADP^+$) in a 96-wells plate. For glucose-6-phosphate determination, the enzymatic conversion was started by addition of 10 μL 10 U/mL glucose-6-phosphate dehydrogenase from yeast (Roche) and $NADP^+$ reduction was followed by measuring NADPH fluorescence at $\lambda_{ex}/\lambda_{em}$ = 320/450 nm in a CLARIOstar microplate reader for 15 min, after which the conversion was complete. Fluorescence changes were calibrated with a NADPH standard of exactly 100 μM as determined by measurement of absorbance at 340 nm. For 6-phosphogluconate determination, the enzymatic conversion was started by addition of 10 μL 0.25 U/mL 6-phosphogluconate dehydrogenase from yeast (Roche) and fluorescence changes were followed for 60 min, after which the conversion was complete.

2.2.8. Measurement of enzyme activities of glucose-6-phosphate dehydrogenase (G6PD) and 6-phosphogluconate dehydrogenase (6PGD)

HepG2 cells were pre-incubated in bicarbonate-free HBSS for 1 h and then treated with 0.1% DMSO or 50 μM LRE1 for 5 min. After the treatment, cells were washed twice in ice-cold PBS and lysed in 200 μL ice-cold lysis buffer (50 mM Tris-HCl pH 8.0, 1 mM EDTA-NaOH, 0.1% (*w*/*v*) Triton X-100, 1× Roche cOmplete protease inhibitor cocktail, and 1× Roche PhosSTOP phosphatase inhibitor cocktail). The lysate was centrifuged at 20,000 ×*g* for 10 min and the supernatant was used for the determination of enzyme activity. The activities of 6PGD and G6PD + 6PGD were measured with saturating concentration of 6-phosphogluconate and glucose-6-phosphate+6-phosphogluconate, respectively. The generated NADPH generated was coupled to reduction WST-1, which regenerates $NADP^+$, avoids allosteric inhibition by NADPH, and allows colorimetric monitoring of the reduced WST-1 at 438 nm in the microplate reader CLARIOstar. Practically, 10 μL lysate was mixed with 150 μL Mixture A (66.7 mM Tris-HCl pH 8.0, 1.33 mM $MgCl_2$, 666.7 μM WST-1 (Dojindo), 13.3 μM 1-Methoxy-5-methylphenazinium methylsulfate (1-Methoxy PMS, Dojindo), and 266.7 μM 6-phosphogluconate) or Mixture B (66.7 mM Tris-HCl pH 8.0, 1.33 mM $MgCl_2$, 666.7 μM WST-1, 13.3 μM 1-Methoxy PMS, 266.7 μM 6-phosphogluconate, and 266.7 μM glucose-6-phosphate) for the determination of 6PDG activity or the combined activity of G6PD and 6PGD, respectively. After measuring the background activity, 50 μL of 50 μM $NADP^+$ was added to start the enzymatic reaction. Enzyme activity was derived from the background-corrected slope (extinction coefficient of reduced WST-1: 37000 M^{-1} cm^{-1}, at 438 nm, pH 8.0) and normalized to protein concentration. G6PD activity was defined as the difference between activities measured in Mixture A and Mixture B. One unit is defined as reduction of 1 μmol WST-1 (equivalent to production of 1 μmol NADPH) per minute at pH 8.0 and 37 °C.

2.2.9. Determination of ATP, ADP, and AMP by high performance liquid chromatography (HPLC) for adenylate energy charges in cytosol

HepG2 cells were treated with 0.1% DMSO or 50 μM sAC-selective inhibitor LRE1 in HBSS containing indicated substrates. After indicated period of incubation, cytosolic metabolites were extracted with permeabilization buffer (120 mM KCl, 10 mM NaCl, 5 mM EDTA, 20 mM HEPES, pH 7.1) containing 100 μg/mL digitonin. After 5 min on ice, 200 μl of digitonin extracts were mixed with 16 μL 70% perchloric acid for deproteinization and then neutralized with 2.5 M K_2CO_3. The neutralized perchloric acid extracts of HepG2 cells were then analyzed for AMP, ADP and ATP by high-performance liquid chromatography using a

Partisphere SAX column (Whatman International Ltd.) exactly as described [30]. Adenylate energy charge was defined as ([ATP] + 0.5 × [ADP])/([ATP] + [ADP] + [AMP]) according to Atkinson and Walton [31].

2.2.10. Cyclic AMP accumulation assay

H69 cholangiocytes were cultured in 24-well plates. Cells were allowed to equilibrate with experimental medium (5% CO_2 DMEM with 5.5 mM glucose, but without glutamine or fetal bovine serum) for 1 h and refreshed again with 200 μL experimental medium. Cells were pretreated with sAC-selective inhibitor KH7 or LRE1 (by adding 25 μL 10× solution) for 10 min and then 500 μM 3-isobutyl-1-methylxanthine (by adding 25 μL 10× solution) was added to induce accumulation of cAMP. After an incubation of 10 min, the accumulation of cAMP was terminated by adding 100 μL 0.35 M HCl/3.5% Triton X-100. The acidic homogenate was centrifuged at 20,000 ×*g* for 10 min at 4 °C to remove cell debris. The cAMP content in the supernatant was measured by the Direct cAMP ELISA kit (Enzo Life Sciences). Although the anti-cAMP antibody only cross-react very slightly with adenylate nucleotides (0.33% with AMP and 0.12% with ATP according to the manufacturer), the concentration of these adenylate nucleotides are typically orders of magnitude higher than that of cAMP. Therefore, the baseline values (obtained without IBMX addition) are considered as assay backgrounds.

2.2.11. SDS-PAGE and Western blotting

Protein concentrations of whole cell lysates in RIPA buffer were quantified by BCA assay. Equal amount of protein (40–50 μg) was subjected to SDS-PAGE, transferred to PVDF membranes by semi-dry blotting and blocked overnight in 5% non-fat milk / PBST (phosphate-buffered saline with 0.05% (*w/v*) Tween 20) at 4 °C. For immunodetection, the PVDF membranes were incubated with primary antibody for 1 h, washed 3 times with TBST (Tris-buffered saline with 0.05% (w/v) Tween 20), incubated with horseradish peroxidase-conjugated secondary antibody for 1 h, and washed again 4 times with TBST. All antibodies were diluted in 1% non-fat milk-TBST and incubation was performed at room temperature. The PVDF membrane was developed with home-made enhanced chemiluminescence reagents (100 mM Tris-HCl pH 8.5, 1.25 mM luminol, 0.2 mM p-coumarin and freshly added 3 mM H_2O_2) and detected using the ImageQuant LAS 4000 (GE Healthcare Life Sciences). Please refer to Supplementary Table 2 for the list of primary and secondary antibodies and dilutions used. Please refer to Supplementary Materials for full blots.

2.2.12. Ratiometric fluorescence measurement for cytosolic free NADPH with iNap biosensor

HepG2 cell lines stably expressing inducible NADPH sensor iNap1 (pCW-iNap1-BSD) or its pH control iNapc (pCW-iNapc-BSD) were cultured in 96-well solid black plates (Costar 3916). Prior to the experiment, cells were treated with 0.8 μg/mL doxycycline for 3 days to induce the expression of iNap1 and iNapc. Experiments were performed in bicarbonate-free HBSS supplemented with 0.1% BSA and 5.5 mM glucose at 37 °C. Fluorescence of iNap and iNapc were monitored by dual excitation ratiometric fluorescence measurement at F_{420} ($\lambda_{Ex1}/\lambda_{Em1}$ = 420–20/540–50 nm) and F_{485} ($\lambda_{Ex2}/\lambda_{Em2}$ = 485–10/540–50 nm) in the microplate reader CLARIOstar. The F_{420}/F_{485} ratio of iNap1 increases with cytosolic NADPH concentration. To correct for potential artifacts due to changes of intracellular pH, changes in the F_{420}/F_{485} ratio of iNap1 were corrected for changes in the F_{420}/F_{485} ratio of iNapc as described [22]. We did not observe changes in iNapc signals after the addition of the compounds used in the experiments.

2.2.13. Ratiometric fluorescence measurement of cytosolic free [NADH]/[NAD$^+$] ratio with Peredox-mCherry biosensor

HepG2 cell lines stably expressing inducible Peredox-mCherry NADH/NAD$^+$ redox sensor (pCW-Peredox-mCherry-BSD) or an empty vector (pCW-MCS-BSD) were cultured in clear-bottomed 96-well black plate (Costar 3603). Cells were induced with 0.8 μg/mL doxycycline for 48 h before the experiment. Experiments were performed in bicarbonate-free HBSS modified in ambient air at 37 °C, supplemented with 0.1% bovine serum albumin (BSA) and indicated substrates at 37 °C. Fluorescence of Peredox (F_1) and mCherry (F_2) was monitored at $\lambda_{Ex1}/\lambda_{Em1}$ = 400–20/535–70 (nm) and $\lambda_{Ex2}/\lambda_{Em2}$ = 570–20/645–80 (nm), respectively, in the CLARIOstar microplate reader. Responsiveness of the Peredox-mCherry sensor was confirmed in each experiment with a series of redox clamping solutions: 5 mM L-lactate, 5 mM pyruvate, and 5 mM L-lactate/pyruvate mixture at a ratio of 1, 5, 10, 20, 50, and 100. Signals from cells transduced with the empty vector (F_1' and F_2' for Peredox channel and mCherry channel, respectively) served to correct for background signals. Background-corrected fluorescence ratio R was defined as $(F_1 - F_1')/(F_2 - F_2')$. For normalization, R was linearly transformed by setting the minimal fluorescence ratio R_{min} (5 mM pyruvate) to 1 and the maximal fluorescence ratio R_{max} (5 mM L-lactate) to 2. Consequently, fluorescence was normalized as $R_{Peredox/mCherry} = (R - R_{min}) / (R_{max} - R_{min}) + 1$. For the comparison of the calibrations using 5 mM and 10 mM [L-Lactate + Pyruvate], the raw fluorescence ratio $R_{Peredox/mCherry}$ was shown in Fig. 3G.

2.2.14. Measurement of mitochondrial membrane potential with JC-1

Mitochondrial membrane potential was measured by the membrane potential-sensitive dye JC-1 [32]. H69 cholangiocytes and HepG2 cells were cultured in clear-bottomed 96-well black plates (Costar 3603). Before experiments, cells were washed and pre-incubated in HBSS modified for 5% CO_2 supplemented with 5.5 mM glucose and 0.2% BSA. After 10 min incubation with vehicle control (0.1% DMSO) or compounds (50 μM KH7, 50 μM LRE1, 2.5 μM antimycin A, 2.5 μM oligomycin A), a ten-fold working solution of JC-1 (by diluting 1 mM DMSO stock in assay medium, Invitrogen) was added to achieve a final concentration of 1 μM. After 20 min incubation with JC-1, the fluorescence signals of JC-1 monomers ($F_{monomer}$) and J-aggregates ($F_{J\text{-}aggregate}$) were measured at $\lambda_{Ex1}/\lambda_{Em1}$ = 490–10/535–10 (nm) and $\lambda_{Ex2}/\lambda_{Em2}$ = 535–20/595–30 (nm), respectively, in the CLARIOstar. The fluorescence ratio ($F_{J\text{-}aggregate}$ / $F_{monomer}$) is an indicator of the mitochondrial membrane potential. Antimycin A dissipates the mitochondrial membrane potential while Oligomycin A causes the mitochondrial membrane potential to increase. These inhibitors served as assay controls and defined the physiologically relevant range of the fluorescence ratio ($F_{J\text{-}aggregate}$ / $F_{monomer}$). The raw fluorescence ratios were normalized to the vehicle control (set to 1).

2.2.15. Extracellular flux analysis

Extracellular acidification rate (ECAR) and oxygen consumption rate (OCR) were measured with a Seahorse XF96 flux analyzer (Agilent, United States) in ambient air. Cells were cultured in a 96-well Seahorse culture plate until confluence in 5% CO_2 incubator. Media were refreshed the day before the experiment. On the day of the experiment, cells were incubated for 1 h in experimental medium in ambient air. For HepG2 cells, the medium was bicarbonate-free HBSS with 5.5 mM glucose (see Supplementary Table 1). For H69 cholangiocytes, the medium was base DMEM (Sigma D-5030) supplemented with 17.8 mM NaCl, 20 mM HEPES-NaOH (pH 7.4), and 5.5 mM glucose. Cells were refreshed with the same medium immediately before determination of ECAR and OCR. Twenty-five microliters of concentrated compound solutions prepared in experimental medium were injected as indicated. The final concentrations of compounds were as follows: indicated compounds (0.1% DMSO, 50 μM LRE1, 50 μM (*R*)-CE3F4, 10 μM ESI-05, 10 μM H89); oligomycin A, 1.6 μM; FCCP, 1.1 μM; antimycin A, 4.62 μM; rotenone, 2.31 μM. The coupled respiration rate was defined as the difference between the average of the first three OCR measurements after the addition of inhibitors or vehicle control and the last OCR measurement after the addition of oligomycin A. The FCCP-driven respiration rate was defined as the difference between the first OCR measurement after FCCP addition and the last OCR measurement after

the addition of oligomycin A.

2.2.16. Estimation of ATP production by glycolysis and by mitochondria using extracellular flux measurements

The time-lapsed ATP production rates were calculated from extracellular fluxes (ECARs and OCRs) as described by Mookerjee et al. [33,34]. Since cells were pre-incubated in HBSS with glucose until reaching steady state before imposing the acute perturbation of sAC activity, it was assumed that the oxidation of the provided substrates in the mitochondria was complete and that the contribution from other endogenous substrates was negligible. The total ATP production rate (J_{ATP_total}) is defined as the sum of the ATP production rate of glycolysis ($J_{ATP\_glycolysis}$, substrate level phosphorylation by phosphoglycerate kinase and pyruvate kinase) and the ATP production rate of mitochondria ($J_{ATP\_mitochondria}$, substrate level phosphorylation by succinyl-CoA synthetase in the TCA cycle and oxidative phosphorylation by the electron transport chain and ATP synthase). To calculate $J_{ATP\_glycolysis}$, it is necessary to distinguish the proton production by glycolysis from that of mitochondrial respiration (as a result of hydration of CO_2). For this purpose, the total proton production rate at measurement time t, $PPR_{total}(t)$, is derived from ECAR by the following equation:

$$PPR_{total}(t) = ECAR(t) \times V \times B$$

where ECAR(t) is the ECAR at measurement time t, V is the volume of the measurement micro-chamber (2 μL for Seahorse XFe96 flux analyzer), and B is the buffer capacity of the experimental medium. Since the experimental medium was buffered with 20 mM HEPES-NaOH (pH 7.4), the contribution of other salt components to buffer capacity was negligible. Taken the value of 7.31 as the pK_a of HEPES at 37 °C and an assay pH of 7.35, the buffer capacity B (M/pH) of the experimental medium was calculated to be 1.31×10^{-2} M/pH according to the definition of the buffer capacity [35]:

$$B = \frac{dC_b}{d(pH)} = ln10\left(\frac{K_w}{[H^+]} + [H^+] + [X]_T \times \frac{K_a[H^+]}{(K_a + [H^+])^2}\right)$$

where C_b represents the normality of the added base, $[X]_T$ represents the concentration of buffer, K_w represents ionization constant of H_2O, and K_a represents the acid dissociation constant of the buffer.

The proton production rate of mitochondrial respiration (PPR_{mito}) and glycolysis (PPR_{gly}) at measurement time t is calculated as follows:

$$PPR_{total}(t) = PPR_{gly}(t) + PPR_{mito}(t)$$

$$PPR_{mito}(t) = OCR_{mito}(t) \times (max H^+/O_2) \times \frac{[HCO_3^-]}{[CO_2] + [HCO_3^-]} = OCR_{mito}(t) \times (max H^+/O_2) \times \frac{10^{pH-pK_{a1}}}{1 + 10^{pH-pK_{a1}}}$$

$$PPR_{gly}(t) = PPR_{total}(t) - PPR_{mito}(t)$$

where max H^+/O_2 is the maximal proton production per O_2 molecule consumed, and pK_{a1} is the combined equilibrium constant (6.093 at 37 °C) for the hydration of CO_2 and the dissociation of H_2CO_3. The OCR_{mito} (needed for the calculation of PPR_{mito}) and $OCR_{coupled}$ (needed for the calculation of $J_{ATP\_mitochondria}$) at measurement time t are derived from the measured OCR, OCR(t), as follows:

$$OCR_{mito}(t) = OCR(t) - OCR_{A+R}$$

$$OCR_{coupled}(t) = (OCR(t) - OCR_{OA}) \times \frac{1}{1 - H}$$

where OCR_{OA} and OCR_{A+R} are the last of the three OCR measurements after the addition of oligomycin A and the combination of antimycin A and rotenone, respectively. Because oligomycin A increases the mitochondria membrane potential, proton leak and the associated oxygen consumption will increase. This will lead to an underestimation of the coupled OCR. Therefore, a correction for hyperpolarisation is included, where H represents the percentage of underestimation and is taken to be 9.2% according to Affourtit and Brand [36]. The $OCR_{coupled}$ for all measurements after the addition of oligomycin A was assumed to be zero. Finally, the ATP production rates J_{ATP_total}, $J_{ATP\_glycolysis}$, J_{ATP_oxphos}, J_{ATP_TCA}, and $J_{ATP\_mitochondria}$ at measurement time t were calculated as follows:

$$J_{ATP\_total}(t) = J_{ATP\_glycolysis}(t) + J_{ATP\_mitochondria}(t)$$

$$J_{ATP\_glycolysis}(t) = PPR_{gly}(t) \times ATP/lactate + 2 \times OCR_{mito}(t) \times P/O_{gly}$$

$$J_{ATP\_mitochondria}(t) = J_{ATP_{oxphos}}(t) + J_{ATP\_TCA}(t)$$

$$J_{ATP\_oxphos}(t) = OCR_{coupled}(t) \times P/O_{oxphos}$$

$$J_{ATP\_TCA}(t) = OCR_{mito}(t) \times P/O_{TCA}$$

where ATP/lactate represents the ATP production per lactate produced. With glucose as the substrate, ATP/lactate is 1. The lactate production rate is assumed to be equal to PPR_{gly}. The values of max H^+/O_2, ATP/lactate, P/O_{gly}, P/O_{oxphos}, and P/O_{TCA} for glucose were taken from the works of Mookerjee et al. [33,34]; these values are given in Supplementary Table 3.

2.2.17. Flux analysis of digitonin-permeabilized cells by Seahorse XFe96 flux analyzer

Cells were pre-incubated in a 96-well Seahorse culture plate in bicarbonate-free HBSS with 5.5 mM glucose and 0.1% (*w/v*) fatty acid-free BSA for 30 min at 37 °C in ambient air. Subsequently, 50 μM LRE1 or 0.1% DMSO (vehicle control) was added. After 20 min incubation, the media in all wells were replaced by MAS buffer (60 mM sucrose, 200 mM mannitol, 10 mM potassium phosphate buffer, 5 mM $MgCl_2$, 1 mM EGTA, 20 mM HEPES and 0.4% fatty acid-free BSA, pH 7.2) as described by Salabei et al. [37] with the same substrates and inhibitors as added during the pre-incubation. The plate was then loaded onto the Seahorse XF96 Analyzer and the measurement started after a 20-min temperature equilibration. Cells were permeabilized with 25 μg/mL digitonin by injecting a concentrated mixture after baseline measurements. The injection mixture also contained substrates for mitochondrial respiration and 1 mM ADP or 2 μM FCCP (final concentration). The final concentrations of substrates were 2 mM pyruvate with 1 mM malate, or 5 mM glutamate with 1 mM malate. Other substrates tested were 5 mM succinate with 2.5 μM rotenone, 0.5 mM durohydroquinone (also known as tetramethyhydroquinone, TCI Europe, Switzerland) and 0.1 mM *N*,*N*,*N*′,*N*′-Tetramethyl-*p*-phenylenediamine (TMPD) with 0.5 mM ascorbate. When substrates were omitted, oxygen consumption decreased dramatically, confirming the oxygen consumption depends on provided substrates. After about 15 min of ADP-driven state 3 respiration, oligomycin A (2.5 μM), and antimycin A (2.5 μM) plus rotenone (1 μM) were injected in order. In some experiments with glutamate plus malate as substrates, a fourth injection contained TMPD plus ascorbate was injected to evaluate complex IV activity. The ADP-driven respiration rate was defined as the difference between the first OCR measurement after the addition the mixture of digitonin, ADP, and substrates and the last OCR measurement after the addition of oligomycin A. The FCCP-driven respiration rate was defined as the difference between the first OCR measurement after FCCP addition and the last OCR measurement after the addition of antimycin A and rotenone.

2.2.18. Spectrophotometric assay for mitochondrial electron transport chain complexes and citrate synthase

Mitochondria were isolated from 30 million HepG2 cells following previously published procedures for cultured fibroblasts [38]. Directly before the enzyme activity measurements of OXPHOS complexes and

citrate synthase, either 1% DMSO, 50 μM LRE1, 1 μM mPKI, or 50 μM CE3F4 was added to the sample. The enzyme assay conditions were as described previously [39].

2.2.19. Statistical analysis

All results are presented as mean ± standard deviation (SD). All *n* numbers refer to the numbers of independent wells of the presented experiments. The number of Independent reproduction is given by N. Statistical analysis was performed with GraphPad Prism 7 (GraphPad Software, La Jolla, CA) with an α error of 0.05. A statistical trend is defined as a *P*-value between 0.05 and 0.07. The types of statistical analysis were decided on the basis of the experimental design and are indicated in the figure legends. Please refer to Supplementary Materials for statistical summaries of all statistic tests performed in this study.

3. Results

3.1. The bicarbonate-responsive soluble adenylyl cyclase (sAC) is highly expressed in human cholangiocyte H69 cells

Although sAC is expressed in most (if not all) tissues and cell lines examined thus far, its low endogenous expression (except in testes) imposes difficulties on the validation of pharmacological and genetic interventions [11]. We have demonstrated previously that the immortalized human intrahepatic cholangiocyte cell line H69 (hereafter H69 cholangiocytes) [23] has high endogenous sAC activity and high expression of sAC protein using the first-generation sAC-selective inhibitor KH7 and lentiviral shRNA-mediated knockdown, respectively [24]. Therefore, in the present metabolic study, the pharmacological and genetic interventions were first validated in H69 cholangiocytes and then applied to H69 cholangiocytes and other cell types for metabolic studies.

Consistent with previous studies, both the first generation sAC-selective inhibitor KH7 [40] and the second generation sAC-selective inhibitor LRE1 [41] significantly suppressed cAMP production in H69 cholangiocytes (Fig. 1A and B). Lentivirus-delivered sAC-targeting shRNA effectively reduced sAC protein level as demonstrated by immunoblotting (Fig. 1C).

3.2. Suppression of soluble adenylyl cyclase stably reprograms cell metabolism towards aerobic glycolysis

Since sAC has been shown to be a physiological ATP sensor [8] and C1-sACKO MEFs displayed increased proton secretion compared to wild-type MEFs [17], we examined whether sAC activity regulates glycolysis. The addition of sAC-selective inhibitor KH7 or LRE1 elicited a slight

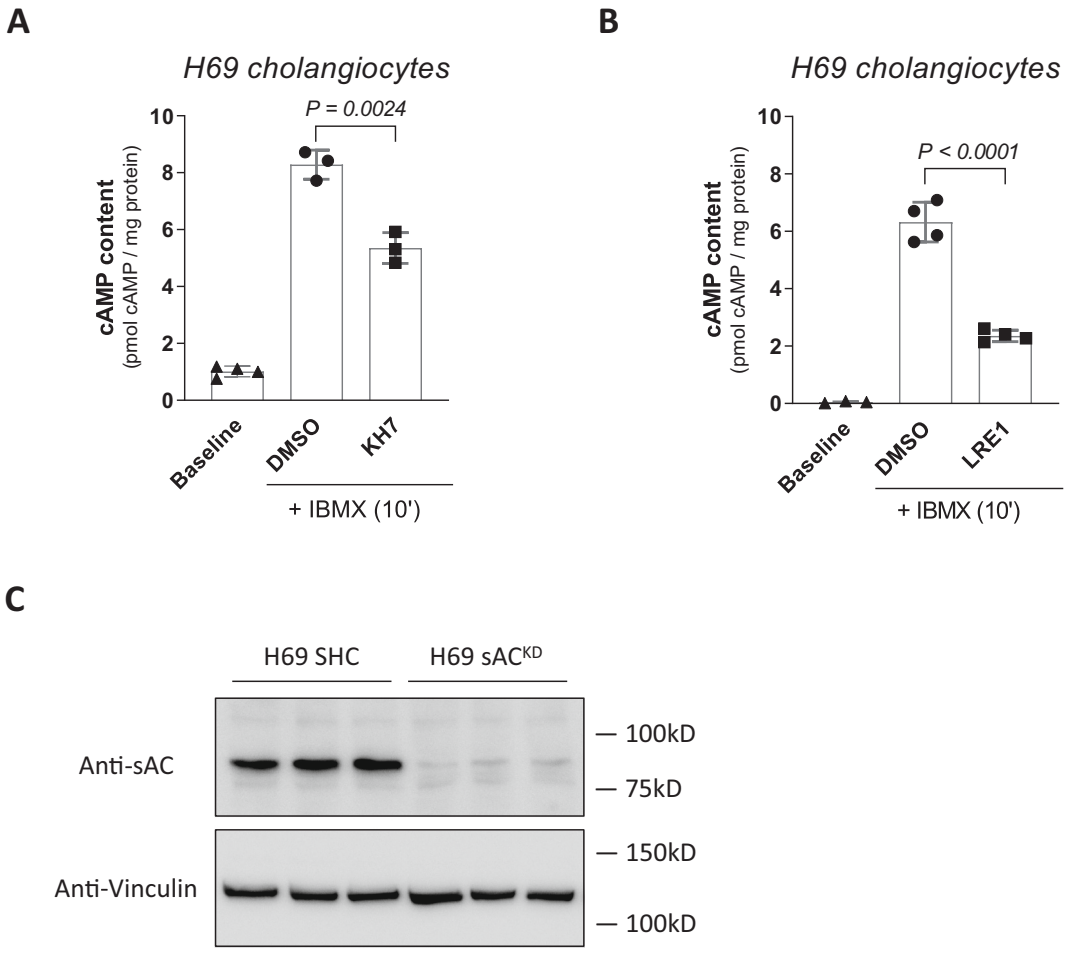

Fig. 1. The bicarbonate-responsive soluble adenylyl cyclase (sAC) is highly expressed in human cholangiocyte H69.
(A–B) sAC activity in H69 was assayed by cAMP accumulation assay in intact cells. H69 cholangiocytes were incubated with in the presence or absence of sAC inhibitor KH7 (A) or LRE1 (B) and then 500 μM IBMX was added to initiate cAMP accumulation. After 10 min, cAMP accumulation was stopped by adding 0.1 M HCl in 1% Triton X-100 (final concentration). The accumulated cAMP was assayed by ELISA. The baseline values obtained before the addition of IBMX serves as assay backgrounds. Data are presented here as mean ± SD ($n = 3$ independent wells for A and $n = 4$ independent wells for B). The results are representative of $N = 3$ independent experiments. Statistical test: unpaired, two-tailed Student's *t*-test. (C) Immunoblot of sAC in H69 cholangiocytes treated with lentivirus-delivered short hairpin control (SHC) and sAC-knockdown shRNA. The result is representative of N = 3 independent experiments.

increase of glucose consumption, but more significantly, there was a dose-dependent increase in lactate secretion and decrease of pyruvate secretion, which resulted in an elevation of the lactate-to-pyruvate ratio in the medium in cells treated with sAC inhibitors (Fig. 2A and S1A). Similarly, acute knockdown of sAC in H69 cholangiocytes also led to increased glucose consumption, increased lactate secretion, but decreased pyruvate secretion. As a consequence, sAC knockdown also increased medium lactate-to-pyruvate ratio (Fig. 2B).

Although we found consistent metabolic changes with both sAC inhibitors (KH7 and LRE1) and sAC knockdown, we also confirmed, in accordance to previous reports by Di Benedetto et al. [13] and Ramos-Espiritu et al. [41], that KH7 collapses the mitochondrial membrane potential while LRE-1 slightly increased the mitochondrial membrane potential in both H69 cholangiocytes and HepG2 cells (Fig. S1B and

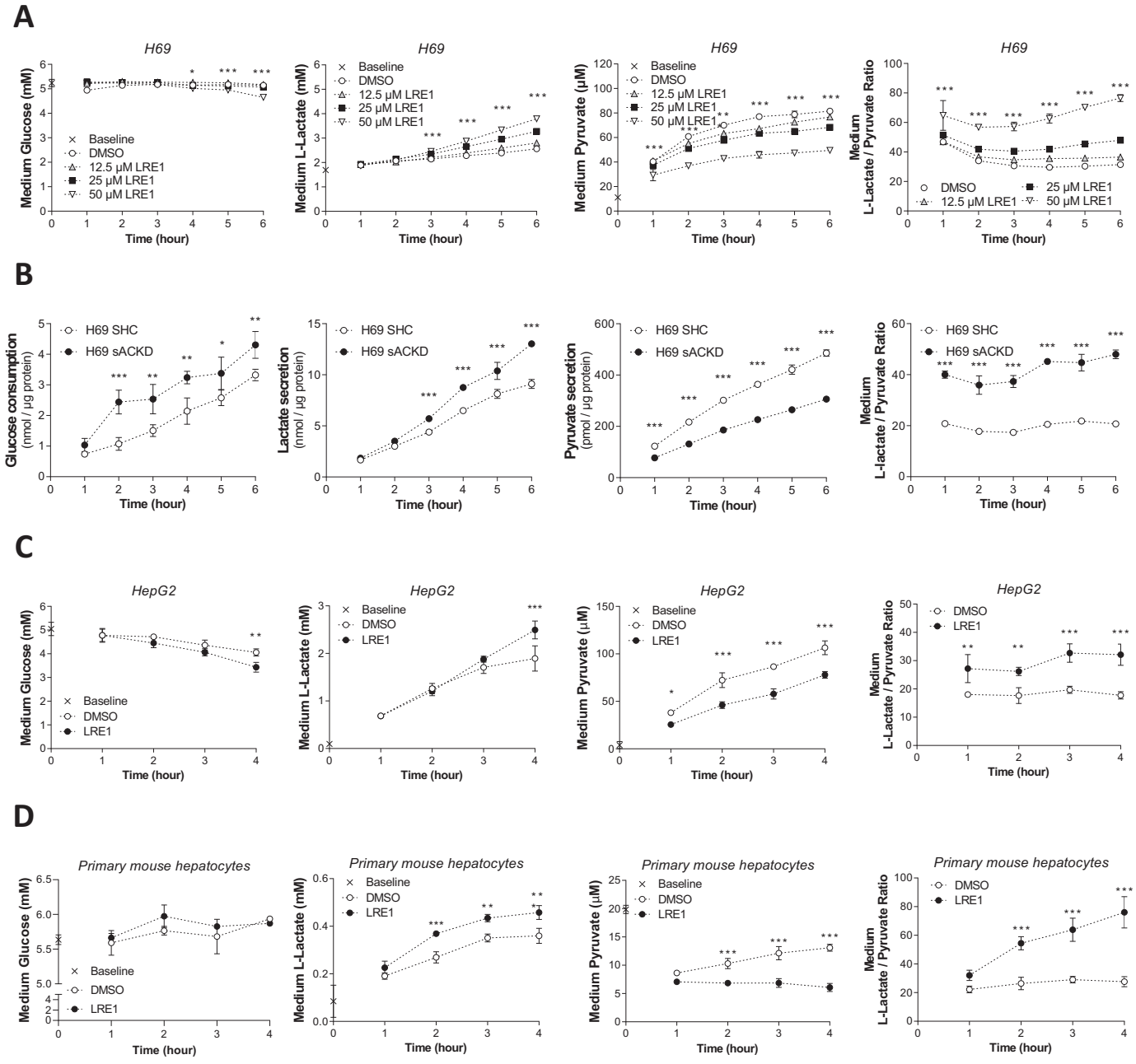

Fig. 2. Suppression of soluble adenylyl cyclase stably reprograms cell metabolism towards aerobic glycolysis.
(A) H69 human cholangiocytes were treated with increasing concentrations of sAC-selective inhibitors LRE1. Medium glucose, L-lactate, and pyruvate were sampled hourly for 6 h and enzymatically determined. Medium L-lactate-to-pyruvate ratio were calculated. (B) Glucose consumption, L-lactate secretion, and pyruvate secretion were determined in SHC and sAC-knockdown H69 human cholangiocytes. The baseline medium glucose was determined to be 5.135 ± 0.062 mM. Medium L-lactate-to-pyruvate ratio was calculated. (C–D) HepG2 cells (C) and primary mouse hepatocytes (D) were treated with sAC-selective inhibitors LRE1. Medium glucose, L-lactate and pyruvate were sampled after 1, 2, 3, and 4 h and enzymatically determined. Data are presented as mean ± SD ($n = 3$ independent wells for A, C, and D; For B, n = 3 independent knockdown by lentivirus transduction). Baseline values present the metabolite concentrations in the blank medium. Data are representative of at least $N = 2$ independent experiments. For some data points, the SD bars are not depicted as they are smaller than the symbols. Statistical analysis: (A) Two-way ANOVA with Tukey's multiple comparisons test. Shown here the statistical significance result of DMSO vs 50 μM LRE1. (B–D) Two-way ANOVA with Sidak's multiple comparisons test. * $P < 0.033$, ** $P < 0.002$, *** $P < 0.001$. Please refer to statistical summaries in Supplementary Materials for complete statistical analysis and exact P values.

S1C). In addition, we found that KH7, but not the second-generation sAC inhibitor LRE1, potently induced hypoxia-inducible factor 1α (HIF-1α) in H69 cholangiocytes (Fig. S1D). To test if sAC suppression can induce HIF-1α protein, we generated stable H69 cholangiocytes that express sAC-targeting shRNA upon doxycycline induction. We found that administration of doxycycline effectively reduced sAC protein level in H69 cholangiocytes in a time-dependent fashion (Fig. S1E) but did not induce HIF-1α (Fig. S1F), suggesting that the induction HIF-1α by KH7 is an off-target effect. Despite of these sAC-independent effects of KH7, inhibiting sAC with KH7 or LRE1 both increased medium lactate-to-pyruvate ratio. However, to avoid misinterpretation of spurious KH7 effects (including uncoupling of mitochondria), we used LRE1 for further metabolic studies.

As sAC is expressed in liver and most other tissues examined [42], we investigated whether sAC also regulates glycolysis in the human hepatoma cell line HepG2 (Fig. 2C), primary mouse hepatocytes (Fig. 2D), primary mouse cholangiocytes (Fig. S2A), primary human cholangiocytes (Fig. S2B), and three additional cell lines of different tissue origin (human colorectal adenocarcinoma Caco-2, Abelson mouse leukemia virus-transformed macrophage RAW264.7, and mouse melanoma cell line B16F10.; Fig. S2C-E). In all cell lines and primary cells tested, inhibition of sAC increased lactate secretion while also reducing pyruvate secretion, which further increased the lactate-to-pyruvate ratio. Although the baseline lactate-to-pyruvate ratios were different in each cell type, sAC inhibition always led to an elevated medium lactate-to-pyruvate ratio. These findings show that sAC-generated cAMP regulates aerobic glycolysis in a great variety of cellular models.

3.3. Soluble adenylyl cyclase regulates the cytosolic NADH/NAD$^+$ redox state

To understand how sAC regulates glucose metabolism, we performed a metabolomics experiment in HepG2 cells fed solely with glucose (Fig. 3A and Supplementary Table 4). Of the intracellular glycolytic intermediates, only glucose-6-phosphate was significantly decreased by sAC inhibition, but there was a trend of increased lactate and decreased pyruvate. We also observed significant changes in metabolites of the pentose phosphate pathway (PPP) (glucose-6-phosphate, 6-phosphogluconate, sedoheptulose-7-phosphate), the Krebs cycle (succinate, cis-aconitate, malate), and malate-aspartate shuttling system (malate, glutamate) and glycerol-3-phosphate shuttling system (glycerol-3-phosphate). The latter two mediate the shuttling of cytosolic NADH into mitochondria for ATP generation. These significant changes suggest that, in addition to glycolysis, sAC inhibition might affect intermediary metabolites of the PPP, the cytosolic NADH/NAD$^+$ redox state, and oxidative phosphorylation.

We first investigated whether sAC regulates flux through the PPP. By direct enzymatic determination, we confirmed that acute sAC inhibition reduced glucose-6-phosphate and 6-phosphogluconate (Fig. S3A and S3B). However, the in vitro activity of the enzymes consuming or generating these metabolites, glucose-6-phosphate dehydrogenase (G6PD) and 6-phosphogluconate dehydrogenase (6PDG), were not affected in cells treated with sAC inhibitors (Fig. S3C). Thus, sAC does not appear to regulate G6PD and 6PDG by covalent modifications (e.g. by phosphorylation/dephosphorylation). In cells, G6PD and 6PGD activities are allosterically inhibited by free NADHP and activated by free NADP$^+$. To assess whether sAC inhibition caused changes in the cytosolic NADPH/NADP$^+$ redox state, we determined the cytosolic free NADPH in HepG2 cells expressing the NADPH biosensor iNap1 [22]. Inhibition of sAC by LRE1 did not significantly affect cytosolic free NADPH level in the presence of glucose even when challenged with diamide, a thiol-oxidizing agent (Fig. S3D and S3E). As a control we showed that when G6PD is inhibited with dehydroepiandrosterone (DHEA), diamide treatment could acutely decrease cytosolic free NADPH. Finally, we asked whether sAC inhibition affects the cytosolic free [NADPH]/[NADP$^+$] ratio, which is in equilibrium with the [Malate]/[Pyruvate] ratio by malic enzyme in the cytosol [43–45]. From the metabolomics data, we observed a significant increase of malate and a trend ($P = 0.067$) towards an increased [Malate]/[Pyruvate] ratio (Fig. 3A and S3F). These data suggest that sAC inhibition does not directly regulate activities of PPP enzymes. Instead, sAC inhibition likely indirectly increases the cytosolic [NADPH]/[NADP$^+$] ratio, thereby allosterically inhibiting G6PD and 6PGD and decreasing levels of the PPP intermediates.

We next focused on the observation that in multiple cell types sAC inhibition increases the medium lactate-pyruvate ratio (Fig. 2 and Fig. S2), which is commonly used as an indicator of the cytosolic NADH/NAD$^+$ redox state [46]. It is well-established that the cytosolic free [NADH]/[NAD$^+$] ratio is equilibrated with the [L-Lactate]/[Pyruvate] ratio by lactate dehydrogenase and, in hepatocytes and muscles, also with the [Glycerol-3-phosphate]/[Dihydroxyacetone phosphate] ratio by cytosolic glycerol-3-phosphate dehydrogenase (GPD1) [46,47]. Therefore, these intracellular metabolites can be used to estimate cytosolic free [NADH]/[NAD$^+$] ratio. In our metabolomics data, we found a significant increase of the [Glycerol-3-phosphate]/[Dihydroxyacetone phosphate] ratio and a trend of an increase of the [L-Lactate]/[Pyruvate] ratio upon sAC inhibition ($P = 0.06$), suggesting an increase in the cytosolic free [NADH]/[NAD$^+$] ratio (Fig. 3B and C). Indeed, direct determination of intracellular pyruvate and lactate confirmed the increase in [Lactate]/[Pyruvate] ratio by the sAC-selective inhibitor LRE-1 in both HepG2 cells and H69 cholangiocytes (Fig. 3D and E). These data strongly suggest that sAC inhibition increases the cytosolic free [NADH]/[NAD$^+$] ratio.

To directly test whether sAC in situ regulates the cytosolic NADH/NAD$^+$ redox state, we expressed the Peredox NADH/NAD$^+$ biosensor [21] in HepG2 cells to detect the ratio of free [NADH] over free [NAD$^+$] in the cytosol (Fig. 3F). The Peredox biosensor responded to altered ratios, but not quantities, of extracellular lactate and pyruvate, confirming that the extracellular lactate-to-pyruvate ratio is in equilibrium with the cytosolic [NADH]/[NAD$^+$] ratio (Fig. 3G). Consistent with the increased lactate-to-pyruvate ratio in medium and in cells, we found that acute inhibition of sAC with LRE1 induced a sustained increase in the cytosolic [NADH]/[NAD$^+$] ratio in the presence of glucose (Fig. 3H). Replacing glucose with the glycolysis inhibitor 2-deoxyglucose reduced baseline cytosolic [NADH]/[NAD$^+$] ratio and completely blocked the increase of [NADH]/[NAD$^+$] ratio induced by sAC inhibition (Fig. 3I). These data demonstrate that cytosolic NADH is maintained by glycolysis and that the increased glycolytic flux contributes to the increased cytosolic [NADH]/[NAD$^+$] ratio under the sAC-suppressed status.

3.4. Soluble adenylyl cyclase regulates cytosolic NADH/NAD$^+$ redox state via complex I

Cytosolic NADH is mainly generated by glycolysis. When there is sufficient oxygen, cytosolic NADH can be shuttled into mitochondria via malate-aspartate shuttling and re-oxidized to NAD$^+$ by complex I. Alternatively, reducing equivalents of cytosolic NADH can be transferred directly to the ubiquinone pool via glycerol-3-phosphate shuttling. When oxidative phosphorylation is impaired, excessive NADH will be oxidized by LDH to regenerate NAD$^+$ with pyruvate being converted to lactate. Therefore, we tested whether sAC inhibition increased the cytosolic [NADH]/[NAD$^+$] ratio and promoted lactate secretion by decreasing NADH oxidation in mitochondria. sAC has been reported to affect different components of the mitochondrial respiratory chain in isolated mitochondria [12,15,16]. We supposed that this could be due to differences in tissue origins, species, and procedures used to isolate mitochondria, and assay condition (e.g. the presence of a phosphatase inhibitor cocktail). To minimize the fragmentation of the mitochondrial networks and local structures during mitochondria isolation, we examined ADP-driven (state 3) respiration and FCCP-driven respiration (with ATP synthase blocked by oligomycin A) in digitonin-permeabilized HepG2 cells using the Seahorse XFe96 Analyzer [37]. When

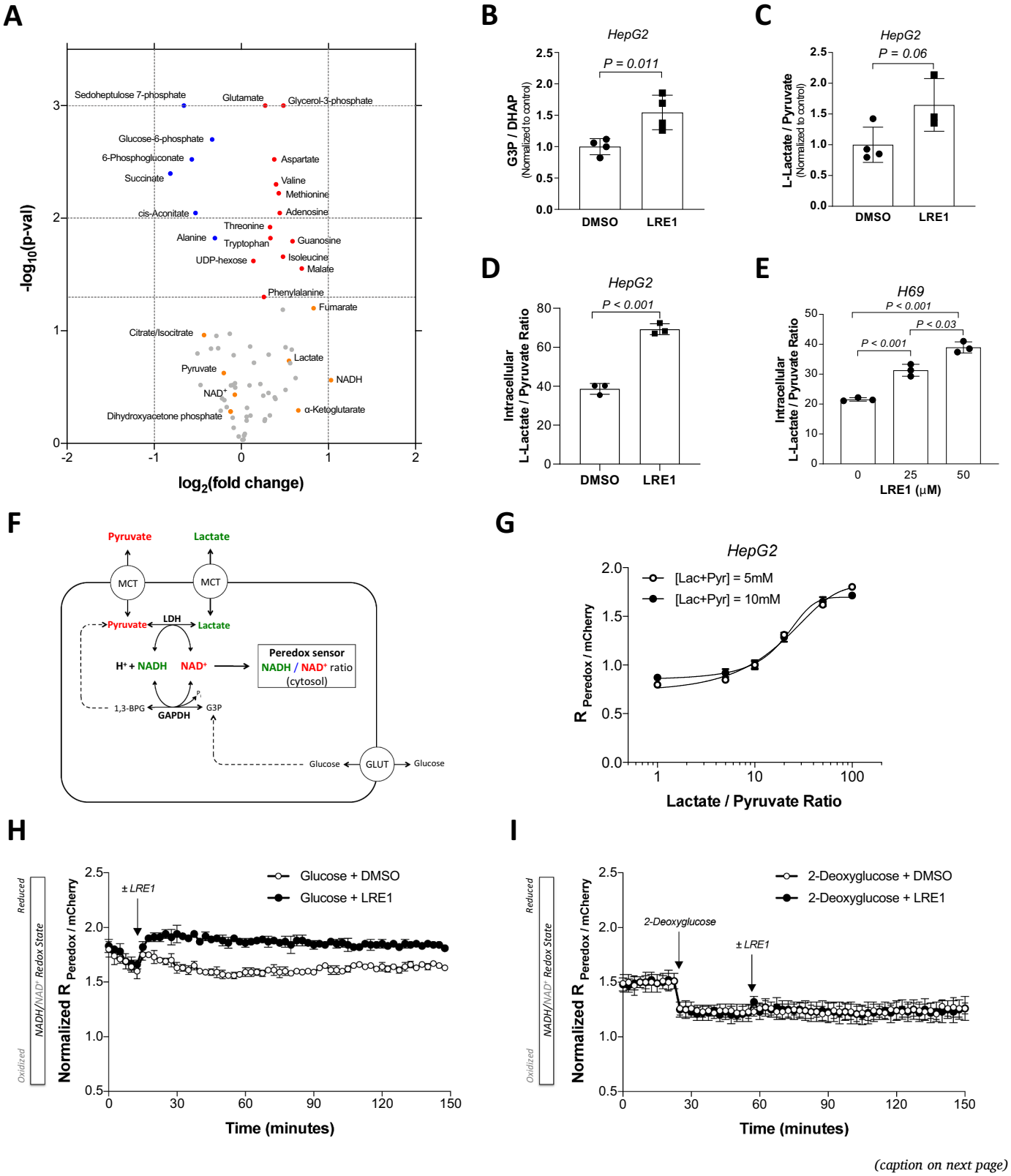

(caption on next page)

Fig. 3. Soluble adenylyl cyclase regulates the cytosolic NADH/NAD^+ redox state.
(A) HepG2 cells were pre-incubated in HBSS with 5.5 mM glucose for 1 h and then treated with the vehicle control (0.1% DMSO) or 50 μM sAC-selective inhibitor LRE1 for 1 h. Intracellular metabolites were determined by untargeted metabolomics from quadruplicate independent samples ($N = 1$ experiment). Data was normalized to the vehicle-treated group and presented by volcano plot. (B–C) Relative intracellular [L-Lactate]/[Pyruvate] ratio (B) and [G3P]/[DHAP] ratio (C) were calculated from the metabolomics data shown in (A). (D) Intracellular lactate-to-pyruvate ratios in HepG2 cells treated with 0.1% DMSO or 50 μM LRE1 for 6 h. Data represent mean ± SD ($n = 3$ independent wells). The result is representative of $N = 3$ independent experiments. (E) H69 cholangiocytes treated with 0.1% DMSO, 25 μM LRE1, or 50 μM LRE1 for 6 h. Data represent mean ± SD (n = 3 independent wells). The result is representative of N = 3 independent experiments. (F) Ubiquitous monocarboxylate transporters (MCTs) equilibrate L-lactate and pyruvate across the plasma membrane. High lactate dehydrogenase activity in most cells brings the substrates (pyruvate and NADH) and products (lactate and NAD^+) to near equilibrium. Therefore, the extracellular lactate-to-pyruvate ratio reflects the cytosolic lactate-to-pyruvate ratio and the cytosolic [NADH]/[NAD^+] ratio. (G) In vivo calibration of the Peredox-mCherry NADH/NAD^+ redox sensor by media with different lactate-to-pyruvate ratio. The raw fluorescence ratio of the redox-sensitive Peredox to tandem-tagged mCherry ($R_{Peredox/mCherry}$) is shown here for the comparison between [L-Lactate + Pyruvate] at 5 mM and 10 mM. (H) HepG2 cells expressing the NADH/NAD^+ redox sensor Peredox-mCherry were incubated with 5.5 mM glucose in HBSS. Fluorescence ratio (R) of the redox-sensitive Peredox to the tandem-tagged mCherry was monitored. Arrow indicates additions of 0.1% DMSO (vehicle control) or 50 μM LRE1. For calibration, cells were incubated with 5 mM lactate and 5 mM pyruvate to obtain maximal (R_{max}) and minimal (R_{min}) ratios, respectively. The results were normalized to R_{max} and R_{min} and presented as mean ± SD ($n = 3$ independent wells). The result is representative of $N = 2$ independent experiments. (G) HepG2 cells expressing the NADH/NAD^+ redox sensor Peredox-mCherry were incubated in glucose-free HBSS. Peredox-mCherry fluorescence were monitored as in (E). Arrows indicate the addition of 5.5 mM 2-deoxyglucose, which was followed by the addition of 0.1% DMSO (vehicle control) or 50 μM LRE1. The results were normalized to R_{max} and R_{min} as in (E) and presented as mean ± SD (n = 4 independent wells). The result is representative of N = 2 independent experiments. Statistical analysis: (A) Multiple *t*-tests. (B–D) Two-tailed unpaired Student's *t*-test. (E) One-way ANOVA with Tukey's multiple comparisons test.

mitochondria were fueled with complex I substrates (i.e., the ubiquinone pool is replenished by NADH oxidation), sAC inhibition strongly and significantly suppressed both ADP-driven and FCCP-driven respiration (Fig. 4A-4C and 4D-4F for pyruvate/malate and glutamate/malate, respectively). However, when mitochondria were fueled with complex II substrate (i.e., the ubiquinone pool is replenished by $FADH_2$ oxidation with succinate as substrate), sAC inhibition only caused a small decrease in ADP-driven respiration and had no effect on FCCP-driven respiration (Fig. 4G-4I). Moreover, we found that sAC inhibition did not suppress ADP-driven respiration using a complex III substrate (durohydroquinone) or a complex IV substrate (TMPD/ascorbate) (Fig. 4J), indicating that sAC does not regulate complex III or complex IV. These data support that sAC primarily regulates complex I-driven respiration. In line with this, inhibiting complex I with a low concentration of rotenone in intact HepG2 cells phenocopied the sAC-suppressed metabolic features, including increased lactate secretion, decreased pyruvate secretion, and elevated medium lactate-to-pyruvate ratio (Fig. S4A-S4C). These results demonstrate in intact cells that sAC regulates the cytosolic NADH/NAD^+ redox state and aerobic glycolysis by controlling complex I-dependent mitochondrial respiration [15,17].

3.5. Soluble adenylyl cyclase regulates complex I-dependent respiration and cytosolic NADH/NAD^+ redox state via Epac1

We next examined which cAMP effector mediated the sAC-dependent regulation of complex I activity and cytosolic NADH/NAD^+ redox state. Since tmAC-derived cAMP and sAC-derived cAMP both use PKA, Epac1, and Epac2 as cAMP effectors, we reasoned that if acute perturbation of tmAC activities did not affect cytosolic NADH/NAD^+ redox state, then by acute, selective inhibition of PKA, Epac1, or Epac2, we can identify the cAMP effectors responsible for sAC-dependent metabolic regulation. To this end, we treated HepG2 cells (Fig. 5A) and H69 cholangiocytes (Fig. 5B) with forskolin (tmAC-selective activator) or 2′,5′-dideoxyadenosine (ddAdo, tmAC-selective inhibitor) both in the absence and presence of sAC-selective-inhibitor LRE1. We found that perturbation of tmAC activities did not acutely affect medium lactate-to-pyruvate ratio, indicating that cAMP generated by tmACs does not acutely regulate cytosolic NADH/NAD^+ redox state. Importantly, the metabolic effect of sAC inhibition was not affected by simultaneous activation or inhibition of tmACs, demonstrating that the cAMP signaling of sAC regulates cellular bioenergetics independently of the cAMP signaling of tmACs.

Since tmAC-dependent cAMP signaling did not regulate the metabolic regulation mediated by sAC, we were able to use selective inhibitors to identify the responsible cAMP effectors of sAC. To this end, we used (*R*)-CE3F4, ESI-05, and myristoylated protein kinase inhibitor 14–22 ($mPKI_{14–22}$) to selectively inhibit Epac1, Epac2, and PKA, respectively (Fig. 5C). The Epac1-selective inhibitor (*R*)-CE3F4 significantly increased medium lactate-to-pyruvate ratio to a comparable level as sAC-selective inhibitor LRE1 in both HepG2 cells (Fig. 5D) and H69 cholangiocytes (Fig. 5E), while inhibition of either Epac2 or PKA had either very small effects or no effect on medium lactate-to-pyruvate ratios. Consistently, in intact HepG2 cells fed with glucose, only inhibition of Epac1 significantly suppressed both ATP-linked OCR and FCCP-uncoupled OCR while inhibition of PKA or Epac2 did not suppress OCR (Fig. 5F-5G and S5A), suggesting sAC regulate cytosolic NADH/NAD^+ redox state via Epac1.

To further confirm our finding, we inhibited PKA and Epac1 in permeabilized HepG2 cells and found that inhibition of Epac1 suppressed both ADP-driven and FCCP-driven complex I respiration using glutamate/malate as substrates (Fig. 5H and I) while having no effect on FCCP-driven complex IV activity using TMPD/ascorbate as substrate. Consistent with lack of effect of PKA-selective inhibition on cytosolic NADH/NAD^+ redox state, PKA-selective inhibitor $mPKI_{14–22}$ had no effect on complex I or complex IV activities. To exclude the possibility that any of the inhibitors we used directly inhibited the mitochondrial electron transport chain or ATP synthase, we purified mitochondria from HepG2 cells, disrupted mitochondrial membranes by combined hypotonic shock and one freeze-thaw cycle, and examined mitochondrial complex activities by spectrophotometric assays in the presence of LRE1, (*R*)-CE3F4, and $mPKI_{14–22}$. Since disrupted mitochondria can no longer produce ATP and GTP, signaling of sAC, PKA, and Epacs were all abolished. As expected, LRE1, (*R*)-CE3F4, and $mPKI_{14–22}$ had no off-target effects on mitochondrial electron transport chain complex activities or ATP synthase activity (Fig. S5B–S5F). Taken together, because tmAC-generated cAMP did not acutely regulate cytosolic NADH/NAD^+ redox state and because only Epac1 inhibition phenocopied the sAC-suppressed metabolic phenotype, our data support that sAC-generated cAMP signals via Epac1 to regulate complex I activity and the cytosolic NADH/NAD^+ redox state.

3.6. Soluble adenylyl cyclase reciprocally regulates glycolysis and oxidative phosphorylation to maintain energy homeostasis

Since sAC has been proposed to be an ATP sensor and we have shown that sAC regulates cytosolic NADH/NAD^+ redox state, glycolysis, and oxidative phosphorylation, we hypothesized that sAC regulates bioenergetic contribution of glycolysis and oxidative phosphorylation to maintain energy homeostasis of cells. To this end, we monitored glycolysis and oxidative phosphorylation simultaneously by measuring the extracellular acidification rate (ECAR) and oxygen consumption (OCR) in a Seahorse Flux Analyzer. In the presence of a physiologic

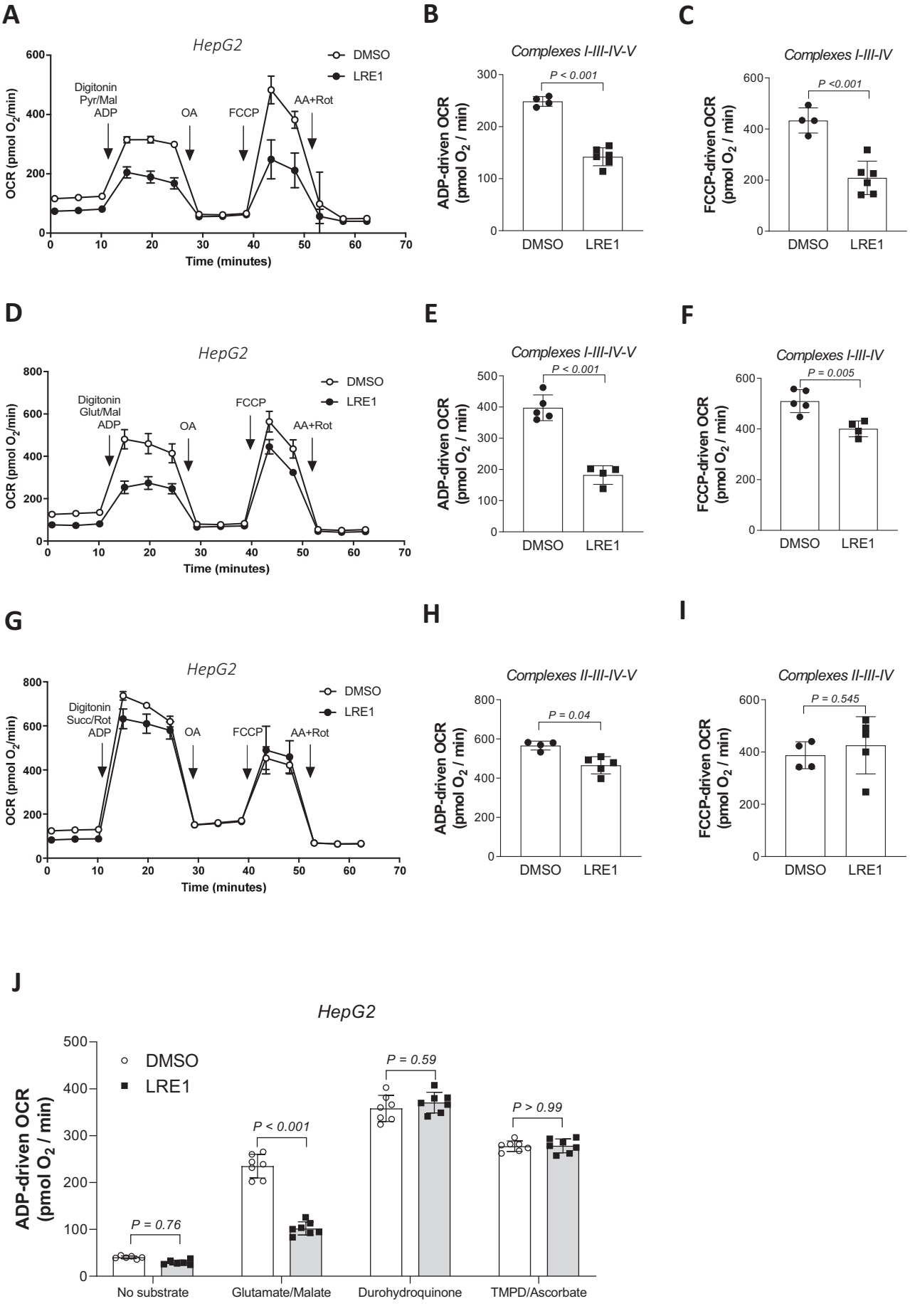

(caption on next page)

Fig. 4. Soluble adenylyl cyclase regulates cytosolic NADH/NAD^+ redox state via complex I.
(A–I) HepG2 cells were pre-treated with 0.1% DMSO or 50 μM LRE1 for 10 min in HBSS and then the medium was changed to MAS buffer with the same compounds. Oxygen consumption rate (OCR) was monitored by the Seahorse XFe96 flux analyzer. Cells were permeabilized by adding 25 μg/mL digitonin together with 1 mM ADP and substrates: (A-C) 2 mM pyruvate and 1 mM malate (n = 4 independent wells for DMSO and *n* = 5 independent wells for LRE1), (D–F) 5 mM glutamate and 1 mM malate (n = 5 independent wells for DMSO and n = 4 independent wells for LRE1) and (G–I) 5 mM succinate and 2.5 μM rotenone (n = 4 independent wells for DMSO and n = 5 independent wells for LRE1). Subsequently, 2.5 μM OA, 1 μM FCCP, and 2.5 μM antimycin A (AA) + 2.5 μM rotenone (Rot) were injected as indicated. (J) HepG2 cells were pre-treated with 0.1% DMSO or 50 μM LRE1 for 10 min in HBSS and then the medium was changed to MAS buffer with the same compounds. Oxygen consumption rate (OCR) was monitored by the Seahorse XFe96 flux analyzer. Cells were permeabilized by adding 25 μg/mL digitonin together with 1 mM ADP and substrates: 5 mM glutamate and 1 mM malate for complex I, 0.5 mM durohydroquinone for complex III, and 0.1 mM TMPD with 0.5 mM ascorbate for complex IV. When no exogenous substrate was added, the OCR was substantially lower. ADP-driven OCR (B, E, H, J) and FCCP-driven OCR (C, F, I) were calculated as described in Methods section. Shown here representative result of $N = 3$ independent experiments for (A)-(I) and N = 2 independent experiments for (J). Statistical analysis: (B–C, E–F, H–I) two-tailed unpaired Student's *t*-test. (J) Two-way ANOVA with Sidak's multiple comparisons test.

concentration of glucose (5.5 mM), inhibiting sAC by LRE1 increased the ECAR and decreased the coupled OCR in both HepG2 cells (Fig. 6A and B) and H69 cells (Fig. S6A and S6B). Importantly, these metabolic effects of sAC inhibition took place within minutes and were sustained. FCCP-uncoupled respiration was also suppressed upon sAC inhibition. To investigate whether energy homeostasis of cells was affected upon inhibition of sAC activity, we derived the ATP production by glycolysis and mitochondria from extracellular flux measurements in intact HepG2 cells following the method described by Mookerjee et al. [33,34] (please refer to 2.2.16 for details). We found that in the presence of glucose, sAC inhibition acutely lowered ATP production by both oxidative phosphorylation and TCA cycle (Fig. 6C-6E) while simultaneously increasing ATP production by glycolysis (Fig. 6F). The overall ATP production remained unchanged (Fig. 6G). Direct determination of adenylate nucleotides in the cytosol also showed no changes in adenylate energy charge (Fig. 6H). Consistently, our metabolomics data also showed that sAC inhibition did not alter the ATP/ADP ratio and the ATP/AMP ratio at the cellular level (Fig. S6C and S6D). These findings demonstrate that sAC maintains cellular energy homeostasis by reciprocally regulating ATP production via glycolysis and oxidative phosphorylation.

4. Discussion

Soluble adenylyl cyclase (sAC), an evolutionarily conserved adenylyl cyclase that senses bicarbonate [2,48], free Ca^{2+} [48,49] and ATP [8], has been proposed to be a metabolic sensor and regulator [6]. Its role in bioenergetics has been studied for more than a decade using isolated mitochondria, but its role in cellular bioenergetics has not been extensively studied [17]. In this work, we provided the first evidence that sAC regulates the cytosolic NADH/NAD^+ redox state, demonstrate that sAC reciprocally regulates glycolysis and oxidative phosphorylation, and established that sAC is an acute bioenergetic regulator at the cellular level. The primary metabolic signature of the sAC-suppressed status, as examined by pharmacological and genetic suppression of sAC, consists of increased glucose consumption, increased lactate secretion, decreased pyruvate secretion, elevated cytosolic [NADH]/[NAD^+] ratio, and suppressed oxidative phosphorylation. Mechanistically, our results suggest that, by regulating complex-I dependent respiration, sAC-generated cAMP controls the cytosolic NADH/NAD^+ redox state while maintaining cellular energy homeostasis. sAC reciprocally tunes ATP production via aerobic glycolysis relative to ATP production by oxidative phosphorylation (Fig. 7). Furthermore, we identified Epac1 as the cAMP effector of sAC for the regulation of complex I-dependent respiration and cytosolic NADH/NAD^+ redox state.

Using the first-generation sAC inhibitor KH7 as well as carbonic anhydrase inhibitor acetazolamide, Acin-Perez et al. were the first to report that mitochondrial sAC senses CO_2/HCO_3^- (which will be primarily Krebs cycle-derived) and stimulates mitochondrial electron transport chain via PKA in mouse liver mitochondria. Their data suggested that sAC regulates complex IV (cytochrome *c* oxidase) activity [50]. Di Benedetto et al. reported that the first-generation sAC inhibitor KH7 negatively affects mitochondrial membrane potential and used an alternative sAC inhibitor, 2-hydroxyestradiol [51], to demonstrate that increased mitochondrial Ca^{2+} uptake via mitochondrial calcium uniporter (MCU) can stimulate mitochondrial sAC to increase the mitochondrial ATP level [13]. Subsequently, De Rasmo et al. reported that sAC regulates complex I and complex IV in mitochondria from human skin fibroblasts [15], but regulates complex IV and complex V (ATP synthase) in mitochondria prepared from rat liver [16]. While both studies used the first-generation sAC inhibitor KH7, carbonic anhydrase inhibitor acetazolamide was also used to indirectly reduce sAC activity by reducing bicarbonate from carbonic anhydrase-mediated CO_2 hydration. Because the non-specific effect KH7 on mitochondrial membranes and its cytotoxicity [13,52], LRE1 was developed as a second-generation sAC-selective allosteric inhibitor a decade later in an independent screening effort by Ramos-Espiritu et al. [41]. In concordance with Di Benedetto et al. [13], we also found that KH7 collapses the mitochondrial membrane potential and importantly, this is not the case with the second generation inhibitor LRE1 [41]. In addition, we found that KH7, but not LRE1 or sAC knockdown, dramatically increases HIF-1α protein level in H69 cholangiocytes under normoxia. These acute and chronic off-target effects of KH7 render this inhibitor unsuitable for mechanistic studies in bioenergetics and metabolism.

The discovery of the second-generation sAC inhibitor LRE1 by Ramos-Espiritu et al. presented a new opportunity to test the observations from the earlier studies [41]. Ramos-Espiritu confirmed that LRE1 suppresses the maximal activity of complex IV in WT mouse embryonic fibroblast (MEF) but not in MEF derived from sAC-C1KO mice [18]. However, the authors did not further characterize the effect of LRE1 on other electron transport chain complexes or on oxidative phosphorylation of intact mitochondria. Valsecchi et al. reported reduced complex I and complex IV activity in freeze-thawed mitochondria prepared from immortalized sAC-C1KO MEFs as compared to WT MEFs [17]. More recently, Jakobsen et al. reported a comprehensive survey using LRE1 and inhibitors of PKA and Epac1 in mitochondria prepared from mouse brain cortex, using the Seahorse XFe96 flux analyzer [53]. They found that inhibition of sAC, PKA, and Epac1 all led to reduced ATP synthesis in isolated mitochondria, suggesting that sAC regulates oxidative phosphorylation via both PKA and Epac1.

The inconsistency in the identification of sAC-regulated targets and cAMP effectors in oxidative phosphorylation among studies could reflect the complex nature of mitochondrial sAC signaling but can also be caused by several factors, including species and tissue origins of the mitochondria, the fragmentation and damage of mitochondria during the isolation procedure and measurement, and the assay conditions (e.g. the presence of a phosphatase inhibitor cocktail will not allow the identification of phosphatase-dependent regulation). To preserve mitochondrial networks and local structures, we studied mitochondrial bioenergetics in digitonin-permeabilized HepG2 cells. We show that the second-generation sAC inhibitor LRE1 suppresses ADP-driven and FCCP-uncoupled complex I-dependent respiration by about 50% when the mitochondria are fueled with complex I substrates (pyruvate/malate and glutamate/malate), but only marginally suppresses ADP-driven respiration and FCCP-uncoupled respiration with complex II substrate succinate (in the presence of rotenone). When mitochondrial was fueled with complex III (durohydroquinone) and complex IV (TMPD/

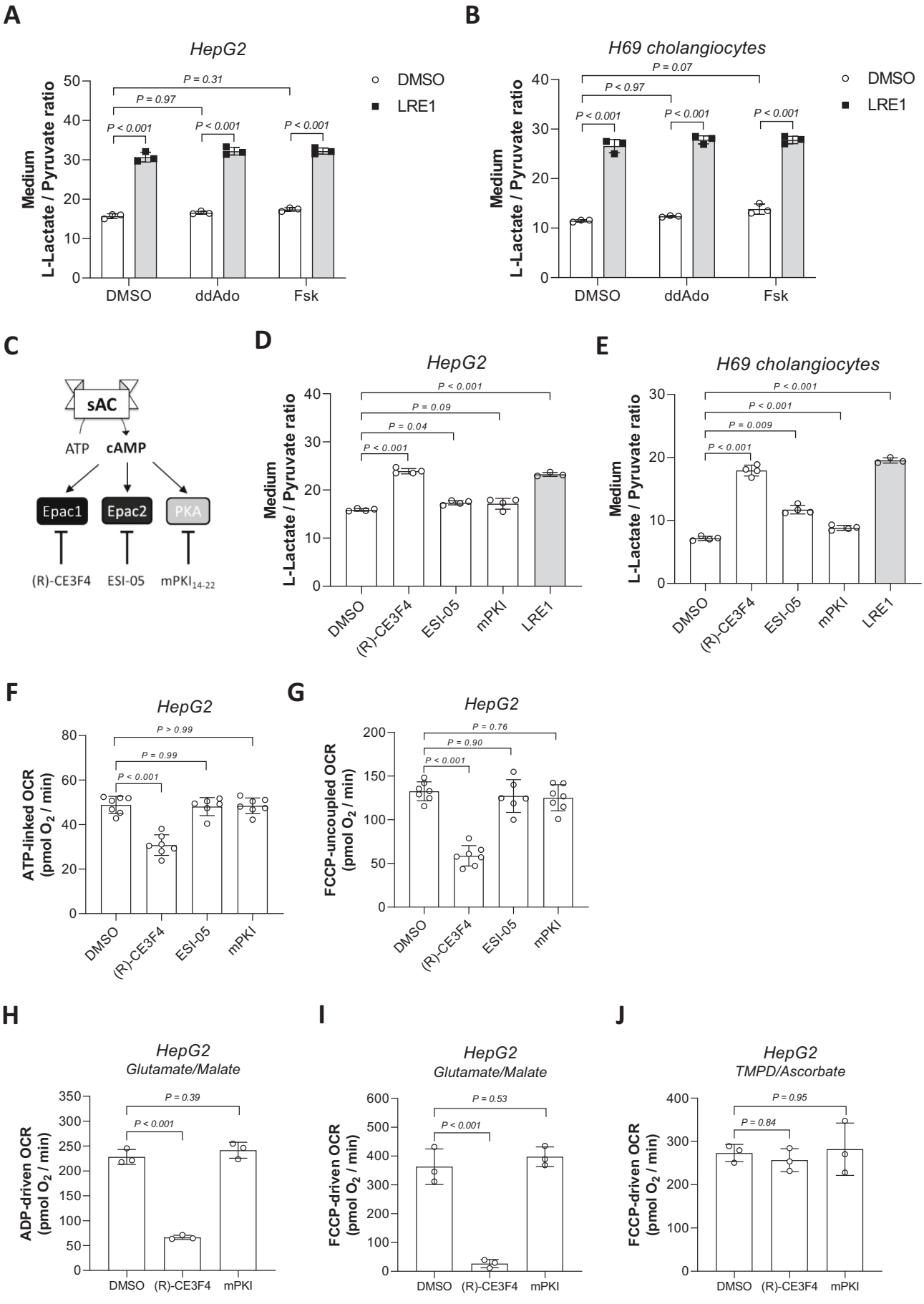

(caption on next page)

Fig. 5. Soluble adenylyl cyclase regulates complex I and cytosolic NADH/NAD^+ via Epac1.
(A–B) HepG2 (A) and H69 cholangiocytes (B) were incubated with DMSO, 50 μM 2′, 5′-dideoxyadenosine (ddAdo, tmAC-selective inhibitor), or 1 μM Forskolin (tmAC-selective activator) in the presence and absence of 50 μM LRE1 (sAC-selective inhibitor) for 1 h in experimental medium containing 5.5 mM glucose. Medium L-lactate and pyruvate were assayed enzymatically to calculate L-lactate-to-pyruvate ratio. Data represents mean ± SD (n = 3 independent wells for all conditions). The result is representative of N = 3 independent experiments. (C) The cAMP effectors Epac1, Epac2, and PKA were selectively inhibited with (*R*)-CE3F4, ESI-05, and myristoylated protein kinase inhibitor peptide 14–22 ($mPKI_{14–22}$), respectively. (D–E) HepG2 cells (D) and H69 cholangiocytes (E) were treated with 0.1% DMSO (vehicle), 50 μM (*R*)-CE3F4, 10 μM ESI-05, 1 μM mPKI, or 50 μM sAC-selective inhibitor LRE1 in experimental medium containing 5.5 mM glucose for 1 hour. Medium lactate and pyruvate were determined to calculate lactate-to-pyruvate ratios. Data represent mean ± SD (n = 3–4 independent wells). The result is representative of N = 3 independent experiments. (F–G) HepG2 cells were pre-incubated in 5.5 mM glucose and oxygen consumption rate was monitored by Seahorse Flux Analyzer. To evaluate the role of Epac1, Epac2, and PKA on mitochondrial oxidative phosphorylation in intact cells, 0.1% DMSO (vehicle control) or selective cAMP effector inhibitors (50 μM (*R*)-CE3F4, 10 μM ESI-05, 1 μM mPKI), oligomycin A (OA), carbonyl cyanide-*p*-trifluoromethoxyphenyl hydrazone (FCCP), and antimycin A (AA) and rotenone (Rot) were injected sequentially. ATP-linked and FCCP-uncoupled OCR were calculated as described in Methods section (see Fig. S5A for full OCR traces). Data represents mean ± SD (*n* = 7, 7, 6, and 7 independent wells for DMSO, (*R*)-CE3F4, ESI-05, and mPKI, respectively). The result is representative of N = 2 independent experiments. (H-J) HepG2 cells were pre-treated with 0.1% DMSO (vehicle control), 50 μM Epac1-specific inhibitor (*R*)-CE3F4, or 1 μM mPKI for 20 min. Cells were then permeabilized with digitonin with 1 mM ADP or 2 μM FCCP with complex-specific substrates: (H) 5 mM glutamate and 1 mM malate, (I) 5 mM glutamate and 1 mM malate, (J) 0.1 mM TMPD and 0.5 mM ascorbate. Shown here the average of N = 3 independent experiments. Statistical analysis: (A–B) Two-way ANOVA with Sidak's multiple comparisons test. (D–J) One-way ANOVA with Tukey's multiple comparisons test.

ascorbate) substrates, sAC inhibition had no effect on ADP-driven mitochondrial respiration. These data do not exclude an inhibition of the F_1/F_O-ATPase as reported by others [16,53] because this enzyme could be without flux control when ADP-driven respiration is supported with complex III or complex IV substrates. Thus, inhibition of the F_1/F_O-ATPase could be the underlying mechanism of the increase in mitochondrial membrane potential induced by sAC inhibition (Fig. S1B and S1C) because in that case fewer protons are transported back via the F_1/F_O-ATPase into the mitochondrial matrix. Of note, in intact HepG2 cells, the second-generation sAC inhibitor LRE1 also suppressed both coupled and uncoupled respiration by about 50%, which is comparable to the results obtained with permeabilized cells. The consistency between data obtained with intact and digitonin-permeabilized cells highlights the importance of preserving mitochondrial network integrity and local structures in bioenergetic studies. While work in isolated mitochondria identified multiple points of sAC-dependent regulation of respiration [15,17,41,50,54], our work suggests that in intact cells a main regulatory function of sAC in oxidative phosphorylation occurs at the level of complex I.

sAC is known to exist in multiple isoforms as a result of an alternative start site [18,42,55,56] and extensive splicing of the mRNA [42,55–58]. In addition to the cytosol [57], sAC isoforms performing different functions have been localized to mitochondria [50,59], nucleus [60,61], microtubules [59], and cilia [56]. Current evidence supports that the specificity of cAMP signaling is maintained by scaffolding adenylyl cyclases, cAMP effectors, and substrates in individual microdomains that are compartmentalized by phosphodiesterases (PDE) [62] or enclosed by cAMP impermeable membranes, such as the mitochondrial inner membrane [13,63]. As such, the specific sAC isoform and its cAMP effector must be localized to the same place. Reports studying sAC in isolated mitochondria identified mitochondrial PKA as the cAMP effector candidate of sAC-mediated regulation of oxidative phosphorylation [15,50,54]. Consistently, our result also support that the cytosolic isoforms are unlikely to be involved in our system because treating cells with forskolin does not affect cytosolic NADH/NAD^+ redox state, as indicated by medium lactate-to-pyruvate ratio (Fig. 5A and B). An important difference between previous reports using isolated mitochondria and our present study is that we identified Epac1 as the primary cAMP effector that regulates complex I-dependent oxidative phosphorylation in permeabilized HepG2 cells while PKA inhibition did not phenocopy sAC-inhibited metabolic phenotype. Of note, in order to avoid the disruption of signaling of cAMP microdomains, the intact cells were treated with inhibitors of sAC, PKA, and Epac1 before digitonin permeabilization in the present study. Therefore, our result represents the summation of the effects of all sAC microdomains and their associated cAMP effectors, including the mitochondrial and membrane-enclosed microdomains.

While Ca^{2+}-sAC-Epac1 signaling has been reported in mitochondria [64–66], Ca^{2+}-mediated activation of sAC is unlikely to be at play in our experimental setting because we did not induce Ca^{2+}-dependent signaling in any of our experiments. In addition, the respiration medium for permeabilized HepG2 cells was free of Ca^{2+} and contained the Ca^{2+} chelator EGTA. In the rat pheochromocytoma cell line PC12 [67] and the human prostate carcinoma cell line LNCaP [68,69], sAC-generated cAMP has been shown to activate Rap. As the known downstream effectors of Epac1, Rap1 and Rap2, are localized to the endosomal system and Golgi apparatus, respectively [70,71], it remains possible that the metabolic regulation by sAC-Epac1 signaling reported here take place in an extra-mitochondrial, membrane-enclosed sAC-Epac1 signaling microdomain. Currently, while most evidence in literature support complex I and (to a lesser extent) complex IV to be candidates regulated by sAC-PKA/Epac1 signaling, the exact molecular mechanism remains to be elucidated. To this end, the identification of the molecular nature and subcellular localization of sAC isoforms, in combination with site-specific expression of constitutive and dominant-negative cAMP effectors, will be necessary to reveal the signaling microdomains of sAC that mediate the metabolic regulation. As the downstream signaling of both PKA and Epac1 involves protein phosphorylation, phosphoproteomics at the subcellular level will be instrumental in elucidating the signaling pathways of sAC isoforms inside and outside mitochondria [72].

In this study, we identified an increased cytosolic [NADH]/[NAD^+] ratio as the metabolic signature of sAC suppression, which is consistent with complex I being a mechanistic target of sAC. Inhibition of complex I (NADH oxidase) leads to an increased mitochondrial [NADH]/[NAD^+] ratio, which allosterically inhibits pyruvate dehydrogenase and three NADH dehydrogenases in the Krebs cycle. In addition, increased mitochondrial [NADH]/[NAD^+] ratio also reduces NADH shuttling from cytosol to mitochondria. As a consequence, the elevated cytosolic [NADH]/[NAD^+] ratio will drive the forward reaction of LDH and result in the characteristic metabolic phenotype of sAC suppression, namely increased lactate secretion and reduced pyruvate secretion (Fig. 7). The reverse of this mechanism was demonstrated in the work of Titov et al., where the lowering of cytosolic [NADH]/[NAD^+] ratio by the water-forming NADH oxidase from *Lactobacillus brevis* increases pyruvate secretion, reduces lactate secretion, reverses aerobic glycolysis, and enhances oxidative phosphorylation [73]. As sAC inhibition increases medium lactate-to-pyruvate ratio in all cell models tested in this study, our results suggest that sAC likely regulates the cytosolic NADH/NAD^+ redox state in a wide variety of cells.

Although we observed no evidence of direct regulation of oxidative PPP enzymes (i.e. G6PD and 6PGD) by sAC, sAC inhibition significantly reduced metabolites in both oxidative PPP (glucose-6-phosphate and 6-phosphogluconate) and non-oxidative PPP (sedoheptulose-7-phosphate). Our data suggest that sAC inhibition likely decreases the oxidative PPP flux by increasing the cytosolic [NADPH]/[$NADP^+$] ratio (which under physiological conditions is already high). Firstly,

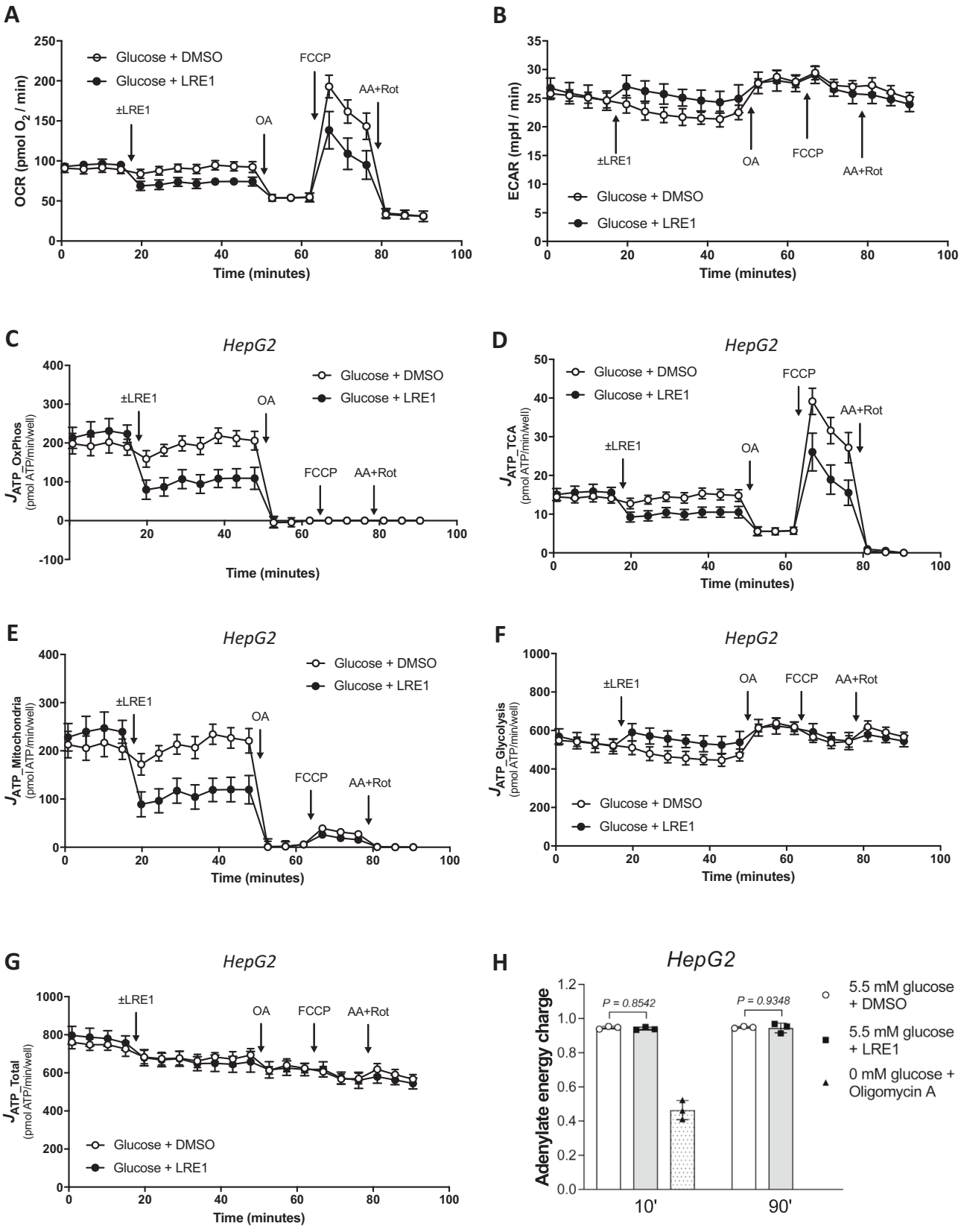

(caption on next page)

Fig. 6. Soluble adenylyl cyclase is an acute switch for aerobic glycolysis that maintains energy homeostasis.
The oxygen consumption rate (OCR) and extracellular acidification rate (ECAR) were analyzed by the Seahorse XFe96 flux analyzer. (A-B) OCR and ECAR of confluent monolayers of HepG2 cells were monitored in HBSS with 5.5 mM glucose. Arrows indicate the injection (in order) of 0.1% DMSO ($n = 10$ independent wells) or 50 μM LRE1 ($n = 9$ independent wells), oligomycin A (OA), carbonyl cyanide-*p*-trifluoromethoxyphenyl hydrazone (FCCP), and antimycin A (AA) and rotenone (Rot). Data are presented as mean ± SD. The result is representative of N = 3 independent experiments. (C-G) ATP production rates by oxidative phosphorylation (J_{ATP_OxPhos})(C), tricarboxylic cycle (J_{ATP_TCA})(D), mitochondria ($J_{ATP\_Mitochondria}$)(E), glycolysis ($J_{ATP\_Glycolysis}$)(F), and total ATP production rate (J_{ATP_Total})(G) were derived from OCR and ECAR measurements in (A) and (B) as described in Methods section. The result is representative of 3 independent experiments. (H) HepG2 cells were treated with 0.1% DMSO (vehicle control) or 50 μM LRE1 for 10 and 90 min. AMP, ADP, and ATP were measured for the calculation of the adenylate energy charge. As a control, cells were also incubated with 2 μM Oligomycin A for 10 min. Data represent mean ± SD (n = 3 independent wells). The result is representative N = 2 independent experiments. Statistical analysis: (H) Two-way ANOVO with Sidak's multiple comparisons test.

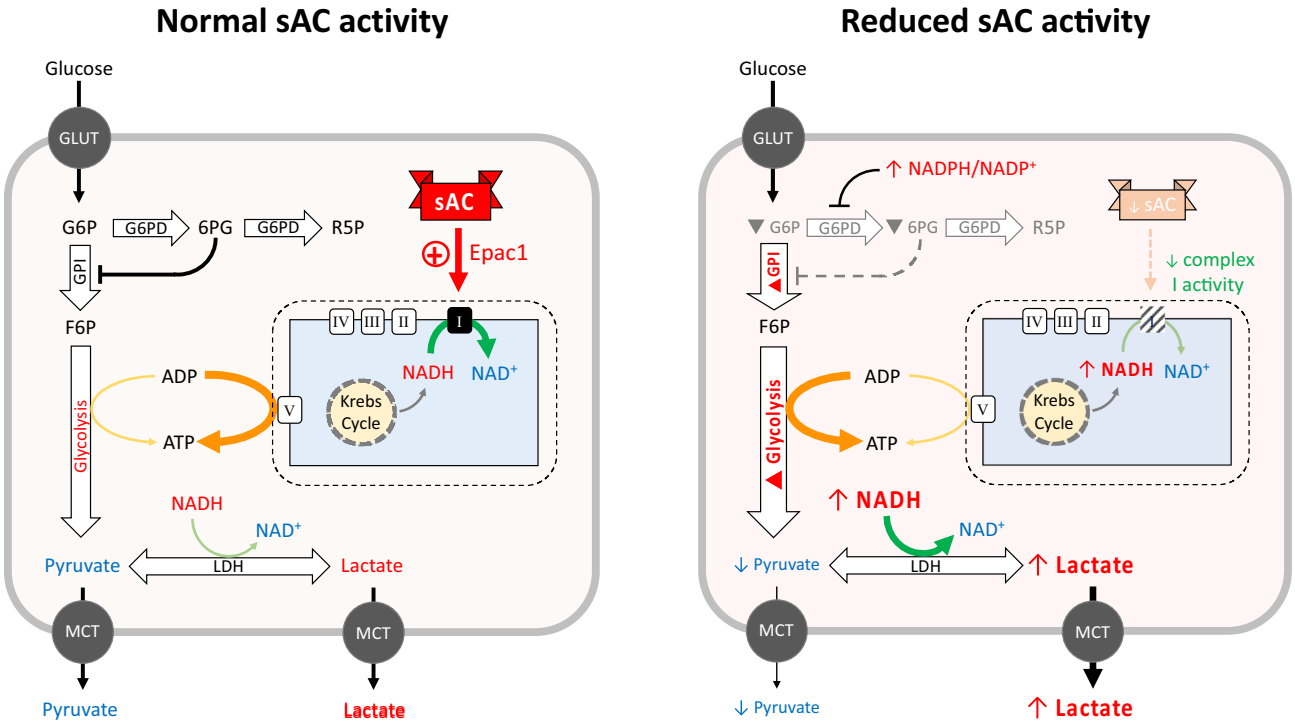

Fig. 7. Working model of the regulation of cellular bioenergetics by sAC-Epac1 signaling.
sAC regulates the complex I (NADH oxidase) of mitochondrial electron transport chain via Epac1. When sAC activity is suppressed, ATP production by oxidative phosphorylation drops acutely. As a consequence, the glycolytic flux increases instantaneously until the ATP deficit is fully compensated, setting a new steady state. Reduced complex I activity increases the mitochondrial [NADH]/[NAD^+] ratio, which decreases the shuttling of cytosolic NADH into mitochondria. The elevated cytosolic [NADH]/[NAD^+] ratio drives the forward reaction of lactate dehydrogenase (LDH), leading to increased lactate secretion and decreased pyruvate secretion. sAC inhibition also indirectly elevates cytosolic NADPH/$NADP^+$ ratio, which allosterically suppresses glucose-6-phosphate dehydrogenase (G6PD) and pentose phosphate pathway flux (PPP). The oxidative PPP metabolite 6-phosphogluconate (6PG) is an established inhibitor of glucose-6-phosphate isomerase (GPI). Decreased level of 6-phosphogluconate (6PG) disinhibits GPI and further increases the production of ATP and NADH by glycolysis.

consistent with complex I inhibition, sAC inhibition increased malate and decreased pyruvate levels, which will increase cytosolic [NADPH]/[$NADP^+$] ratio via the cytosolic malic enzyme [43–45]. Secondly, an increased cytosolic [NADH]/[NAD^+] ratio can also indirectly increase cytosolic [NADPH]/[$NADP^+$] ratio via the equilibrium between LDH and the cytosolic malic enzyme through their common substrate pyruvate [43]. Thirdly, consistent with a reduced PPP flux, sAC inhibition decreases the level of 6-phosphogluconate, a well-established and potent competitive inhibitor of glucose-6-phosphate isomerase (GPI) [74–78]. Parr was the first to report 6-phosphogluconate as a potent inhibitor of GPI in mammalian tissues and suggested that the in vivo activity of GPI is strongly inhibited by the physiological concentration of 6-phosphogluconate despite the high in vitro activity in enzymatic assays [75]. Several subsequent studies demonstrated that both pharmacological and genetic suppression of G6PD activity reduces 6-phosphogluconate and promotes glycolysis [79–81]. Conversely, inhibition of 6PGD by 6-aminonicotinamide increases 6-phosphogluconate and reduces glycolytic flux [82–86]. These studies are consistent with a mechanism whereby sAC inhibition (further) increases the NADPH concentration which (further) inhibits G6PDH and lowers 6-phosphogluconate level to disinhibit GPI, leading to a "pull" mechanism that decreases glucose-6-phosphate and promotes the production of ATP and NADH by glycolysis (Fig. 7).

Finally, the metabolic regulation by sAC is potentially important in physiological and pathological processes associated with an altered balance in ATP production between glycolysis and oxidative phosphorylation, such as cancer metabolism [87,88], proliferation and differentiation of stem cells [89], and activation of macrophages, dendritic cells and T-cells [90]. In particular, the metabolic reprogramming in the sAC-suppressed state, namely increased glycolytic flux and cytosolic [NADH]/[NAD^+] ratio with reduction in oxidative phosphorylation, resembles the seminal observation described by Otto Warburg that growing tumors utilized glucose by aerobic glycolysis despite sufficient oxygen tension for oxidative phosphorylation. This contention is supported by the observation that a large panel of tumor samples have lower sAC expression than the adjacent normal tissues [91]. Moreover, the recent development of NADH/NAD^+ biosensors confirms that transformed cells have in general an elevated cytosolic free [NADH]/

[NAD^+] ratio as compared to non-transformed cells [92,93]. While the Warburg effect in tumor cells is primarily driven by accumulating genetic mutations and epigenetic changes, it can also arise, as this study shows, from altered sAC expression and signaling. The metabolic regulation by sAC can therefore be further explored to manipulate the proliferation of cancer cells and inflammatory responses of macrophages, dendritic cells and T-cells. Finally, the regulation of complex I by sAC connects cAMP signaling to AMPK signaling [17], a master metabolic regulator that regulates fatty acid oxidation, cholesterol synthesis, and glycogen metabolism [94], and couples metabolic signals to the Hippo-YAP (Yes-associated Protein 1, *YAP1*)/TAZ (WW Domain Containing Transcription Regulator 1, *WWTR1*) pathway [95,96]. In line with this, cholesterol was recently shown to promote non-alcoholic steatohepatitis via TAZ in a sAC-dependent manner [97].

5. Conclusions

We demonstrate that the evolutionarily conserved soluble adenylyl cyclase is a master regulator of energy metabolism at the cellular level. By regulating complex I-dependent respiration of mitochondria, sAC coordinates glycolysis, cytosolic NADH/NAD^+ redox state, and oxidative phosphorylation to maintain cellular energy homeostasis. As such, sAC acts as a bioenergetic switch between aerobic glycolysis and oxidative phosphorylation at the post-translational level.

Supplementary data to this article can be found online at https://doi.org/10.1016/j.bbabio.2020.148367.

Declaration of competing interest

Jochen Buck and Lonny Levin own equity interest in CEP Biotech which has licensed commercialization of a panel of monoclonal antibodies directed against sAC. All other co-authors declare no conflict of interest.

The authors declare the following financial interests/personal relationships which may be considered as potential competing interests:

Drs. Jochen Buck and Lonny L. Levin own equity interest in CEP Biotech which has licensed commercialization of a panel of monoclonal antibodies directed against sAC. All other co-authors declare no conflict of interest.

Acknowledgements

Ronald Oude Elferink and Jung-Chin Chang are supported by grant #11652-2018-1 from the Dutch Cancer Society (KWF/Alpe d'HuZes). Jung-Chin Chang is also supported by AGEM Talent development Grant of the Amsterdam Gastroenterology, Endocrinology & Metabolism Research Institute. Jochen Buck and Lonny Levin are supported by NIH grants AG061290 and HD088571. The authors thank Dr. D. de Korte (Sanquin Blood Foundation, Amsterdam, NL) for performing the analysis of adenylate nucleotides and Dr. Michel van Weeghel of the Amsterdam UMC Metabolomics Core for performing and analyzing the metabolomics experiment.

Author contributions

JCC, AJV and ROE developed the study concept. JCC, SG, EHG, SD, HLL, HSH, DMP, RJR, and AJV designed, performed, and analyzed the experiments. JB and LRL provided insights in study design and interpretation. JCC drafted the manuscript. All co-authors commented and reviewed the manuscript and agreed with their authorship.

References

[1] E.W. Sutherland, T.W. Rall, Fractionation and characterization of a cyclic adenine ribonucleotide formed by tissue particles, J. Biol. Chem. 232 (2) (1958) 1077–1091.
[2] Y. Chen, M.J. Cann, T.N. Litvin, V. Iourgenko, M.L. Sinclair, L.R. Levin, et al., Soluble adenylyl cyclase as an evolutionarily conserved bicarbonate sensor, Science 289 (5479) (2000) 625–628.
[3] M. Kamenetsky, S. Middelhaufe, Bank, E.M, L.R. Levin, J. Buck, C. Steegborn, Molecular details of cAMP generation in mammalian cells: a tale of two systems, J. Mol. Biol. 362 (4) (2006) 623–639.
[4] T.N. Litvin, M. Kamenetsky, A. Zarifyan, J. Buck, L.R. Levin, Kinetic properties of "soluble" adenylyl cyclase. Synergism between calcium and bicarbonate, J. Biol. Chem. 278 (18) (2003) 15922–15926.
[5] S. Kleinboelting, A. Diaz, S. Moniot, J. van den Heuvel, M. Weyand, L.R. Levin, et al., Crystal structures of human soluble adenylyl cyclase reveal mechanisms of catalysis and of its activation through bicarbonate, Proc. Natl. Acad. Sci. U. S. A. 111 (10) (2014) 3727–3732.
[6] J.H. Zippin, L.R. Levin, J. Buck, CO(2)/HCO(3)(−)-responsive soluble adenylyl cyclase as a putative metabolic sensor, Trends Endocrinol. Metab. 12 (8) (2001) 366–370.
[7] M. Kobayashi, J. Buck, L.R. Levin, Conservation of functional domain structure in bicarbonate-regulated "soluble" adenylyl cyclases in bacteria and eukaryotes, Dev. Genes Evol. 214 (10) (2004) 503–509.
[8] J.H. Zippin, Y. Chen, S.G. Straub, K.C. Hess, A. Diaz, D. Lee, et al., CO2/HCO3(−)- and calcium-regulated soluble adenylyl cyclase as a physiological ATP sensor, J. Biol. Chem. 288 (46) (2013) 33283–33291.
[9] B.S. Jaiswal, M. Conti, Calcium regulation of the soluble adenylyl cyclase expressed in mammalian spermatozoa, Proc. Natl. Acad. Sci. U. S. A. 100 (19) (2003) 10676–10681.
[10] W. Geng, Z. Wang, J. Zhang, B.Y. Reed, C.Y. Pak, O.W. Moe, Cloning and characterization of the human soluble adenylyl cyclase, Am. J. Phys. Cell Phys. 288 (6) (2005) C1305–C1316.
[11] L.R. Levin, J. Buck, Physiological roles of acid-base sensors, Annu. Rev. Physiol. 77 (2015) 347–362.
[12] R. Acin-Perez, E. Salazar, M. Kamenetsky, J. Buck, L.R. Levin, G. Manfredi, Cyclic AMP produced inside mitochondria regulates oxidative phosphorylation, Cell Metab. 9 (3) (2009) 265–276.
[13] G. Di Benedetto, E. Scalzotto, M. Mongillo, T. Pozzan, Mitochondrial Ca(2)(+) uptake induces cyclic AMP generation in the matrix and modulates organelle ATP levels, Cell Metab. 17 (6) (2013) 965–975.
[14] H. Han, A. Stessin, J. Roberts, K. Hess, N. Gautam, M. Kamenetsky, et al., Calcium-sensing soluble adenylyl cyclase mediates TNF signal transduction in human neutrophils, J. Exp. Med. 202 (3) (2005) 353–361.
[15] D. De Rasmo, A. Signorile, A. Santeramo, M. Larizza, P. Lattanzio, G. Capitanio, et al., Intramitochondrial adenylyl cyclase controls the turnover of nuclear-encoded subunits and activity of mammalian complex I of the respiratory chain, Biochim. Biophys. Acta 1853 (1) (2015) 183–191.
[16] D. De Rasmo, L. Micelli, A. Santeramo, A. Signorile, P. Lattanzio, S. Papa, cAMP regulates the functional activity, coupling efficiency and structural organization of mammalian FOF1 ATP synthase, Biochim. Biophys. Acta 1857 (4) (2016) 350–358.
[17] F. Valsecchi, C. Konrad, M. D'Aurelio, L.S. Ramos-Espiritu, A. Stepanova, S. R. Burstein, et al., Distinct intracellular sAC-cAMP domains regulate ER Ca(2+) signaling and OXPHOS function, J. Cell Sci. 130 (21) (2017) 3713–3727.
[18] J. Farrell, L. Ramos, M. Tresguerres, M. Kamenetsky, L.R. Levin, J. Buck, Somatic 'soluble' adenylyl cyclase isoforms are unaffected in Sacy tm1Lex/Sacy tm1Lex 'knockout' mice, PLoS One 3 (9) (2008), e3251.
[19] J. Moffat, D.A. Grueneberg, X. Yang, S.Y. Kim, A.M. Kloepfer, G. Hinkle, et al., A lentiviral RNAi library for human and mouse genes applied to an arrayed viral high-content screen, Cell 124 (6) (2006) 1283–1298.
[20] T. Wang, J.J. Wei, D.M. Sabatini, E.S. Lander, Genetic screens in human cells using the CRISPR-Cas9 system, Science 343 (6166) (2014) 80–84.
[21] Y.P. Hung, J.G. Albeck, M. Tantama, G. Yellen, Imaging cytosolic NADH-NAD(+) redox state with a genetically encoded fluorescent biosensor, Cell Metab. 14 (4) (2011) 545–554.
[22] R. Tao, Y. Zhao, H. Chu, A. Wang, J. Zhu, X. Chen, et al., Genetically encoded fluorescent sensors reveal dynamic regulation of NADPH metabolism, Nat. Methods 14 (7) (2017) 720–728.
[23] S.A. Grubman, R.D. Perrone, D.W. Lee, S.L. Murray, L.C. Rogers, L.I. Wolkoff, et al., Regulation of intracellular pH by immortalized human intrahepatic biliary epithelial cell lines, Am. J. Phys. 266 (6 Pt 1) (1994) G1060–G1070.
[24] J.C. Chang, S. Go, D.R. de Waart, P. Munoz-Garrido, U. Beuers, C.C. Paulusma, et al., Soluble adenylyl Cyclase regulates bile salt-induced apoptosis in human Cholangiocytes, Hepatology 64 (2) (2016) 522–534.
[25] E.H. Gilglioni, J.-C. Chang, S. Duijst, S. Go, A.A.A. Adam, R. Hoekstra, et al., Improved oxygenation dramatically alters metabolism and gene expression in cultured primary mouse hepatocytes, Hepatology Communications 2 (3) (2018) 299–312.
[26] J.M. Banales, E. Saez, M. Uriz, S. Sarvide, A.D. Urribarri, P. Splinter, et al., Up-regulation of microRNA 506 leads to decreased cl-/HCO3- anion exchanger 2 expression in biliary epithelium of patients with primary biliary cirrhosis, Hepatology 56 (2) (2012) 687–697.
[27] D.A. Blake, N.V. McLean, A colorimetric assay for the measurement of D-glucose consumption by cultured cells, Anal. Biochem. 177 (1) (1989) 156–160.
[28] A. Zhu, R. Romero, H.R. Petty, A sensitive fluorimetric assay for pyruvate, Anal. Biochem. 396 (1) (2010) 146–151.
[29] E.P. Marbach, M.H. Weil, Rapid enzymatic measurement of blood lactate and pyruvate. Use and significance of metaphosphoric acid as a common precipitant, Clin. Chem. 13 (4) (1967) 314–325.

[30] I.J. Bontekoe, P.F. van der Meer, K. van den Hurk, A.J. Verhoeven, D. de Korte, Platelet storage performance is consistent by donor: a pilot study comparing "good" and "poor" storing platelets, Transfusion 57 (10) (2017) 2373–2380.
[31] D.E. Atkinson, G.M. Walton, Adenosine triphosphate conservation in metabolic regulation. Rat liver citrate cleavage enzyme, J. Biol. Chem. 242 (13) (1967) 3239–3241.
[32] S.T. Smiley, M. Reers, C. Mottola-Hartshorn, M. Lin, A. Chen, T.W. Smith, et al., Intracellular heterogeneity in mitochondrial membrane potentials revealed by a J-aggregate-forming lipophilic cation JC-1, Proc. Natl. Acad. Sci. U. S. A. 88 (9) (1991) 3671–3675.
[33] S.A. Mookerjee, A.A. Gerencser, D.G. Nicholls, M.D. Brand, Quantifying intracellular rates of glycolytic and oxidative ATP production and consumption using extracellular flux measurements, J. Biol. Chem. 292 (17) (2017) 7189–7207.
[34] S.A. Mookerjee, R.L.S. Goncalves, A.A. Gerencser, D.G. Nicholls, M.D. Brand, The contributions of respiration and glycolysis to extracellular acid production, Biochim. Biophys. Acta 1847 (2) (2015) 171–181.
[35] E.T. Urbansky, M.R. Schock, Understanding, deriving, and computing buffer capacity, J. Chem. Educ. 77 (12) (2000) 1640–1644.
[36] C. Affourtit, M.D. Brand, Measuring mitochondrial bioenergetics in INS-1E insulinoma cells, Methods Enzymol. 457 (2009) 405–424.
[37] J.K. Salabei, A.A. Gibb, B.G. Hill, Comprehensive measurement of respiratory activity in permeabilized cells using extracellular flux analysis, Nat. Protoc. 9 (2) (2014) 421–438.
[38] A.J. Janssen, F.J. Trijbels, R.C. Sengers, J.A. Smeitink, L.P. van den Heuvel, L. T. Wintjes, et al., Spectrophotometric assay for complex I of the respiratory chain in tissue samples and cultured fibroblasts, Clin. Chem. 53 (4) (2007) 729–734.
[39] R.J. Rodenburg, Biochemical diagnosis of mitochondrial disorders, J. Inherit. Metab. Dis. 34 (2) (2011) 283–292.
[40] K.C. Hess, B.H. Jones, B. Marquez, Y. Chen, T.S. Ord, M. Kamenetsky, et al., The "soluble" adenylyl cyclase in sperm mediates multiple signaling events required for fertilization, Dev. Cell 9 (2) (2005) 249–259.
[41] L. Ramos-Espiritu, S. Kleinboelting, F.A. Navarrete, A. Alvau, P.E. Visconti, F. Valsecchi, et al., Discovery of LRE1 as a specific and allosteric inhibitor of soluble adenylyl cyclase, Nat. Chem. Biol. 12 (10) (2016) 838–844.
[42] W. Geng, Z. Wang, J. Zhang, B.Y. Reed, C.Y. Pak, O.W. Moe, Cloning and characterization of the human soluble adenylyl cyclase, Am. J. Phys. Cell Phys. 288 (6) (2005) C1305–C1316.
[43] R.L. Veech, L.V. Eggleston, H.A. Krebs, The redox state of free nicotinamide-adenine dinucleotide phosphate in the cytoplasm of rat liver, Biochem. J. 115 (4) (1969) 609–619.
[44] M. Zelewski, J. Swierczynski, Malic enzyme in human liver. Intracellular distribution, purification and properties of cytosolic isozyme, Eur. J. Biochem. 201 (2) (1991) 339–345.
[45] C.J. Hedeskov, K. Capito, P. Thams, Cytosolic ratios of free [NADPH]/[NADP+] and [NADH]/[NAD+] in mouse pancreatic islets, and nutrient-induced insulin secretion, Biochem. J. 241 (1) (1987) 161–167.
[46] D.H. Williamson, P. Lund, H.A. Krebs, The redox state of free nicotinamide-adenine dinucleotide in the cytoplasm and mitochondria of rat liver, Biochem. J. 103 (2) (1967) 514–527.
[47] J.T. Barron, L. Gu, J.E. Parrillo, Malate-aspartate shuttle, cytoplasmic NADH redox potential, and energetics in vascular smooth muscle, J. Mol. Cell. Cardiol. 30 (8) (1998) 1571–1579.
[48] T.N. Litvin, M. Kamenetsky, A. Zarifyan, J. Buck, L.R. Levin, Kinetic properties of "soluble" adenylyl cyclase. Synergism between calcium and bicarbonate, J. Biol. Chem. 278 (18) (2003) 15922–15926.
[49] B.S. Jaiswal, M. Conti, Calcium regulation of the soluble adenylyl cyclase expressed in mammalian spermatozoa, Proc. Natl. Acad. Sci. U. S. A. 100 (19) (2003) 10676–10681.
[50] R. Acin-Perez, E. Salazar, M. Kamenetsky, J. Buck, L.R. Levin, G. Manfredi, Cyclic AMP produced inside mitochondria regulates oxidative phosphorylation, Cell Metab. 9 (3) (2009) 265–276.
[51] J.L. Bitterman, L. Ramos-Espiritu, A. Diaz, L.R. Levin, J. Buck, Pharmacological distinction between soluble and transmembrane adenylyl cyclases, J. Pharmacol. Exp. Ther. 347 (3) (2013) 589–598.
[52] E. Jakobsen, S.C. Lange, J.V. Andersen, C. Desler, H.F. Kihl, M.C. Hohnholt, et al., The inhibitors of soluble adenylate cyclase 2-OHE, KH7, and bithionol compromise mitochondrial ATP production by distinct mechanisms, Biochem. Pharmacol. 155 (2018) 92–101.
[53] E. Jakobsen, S.C. Lange, L.K. Bak, Soluble adenylyl cyclase-mediated cAMP signaling and the putative role of PKA and EPAC in cerebral mitochondrial function, J. Neurosci. Res. 97 (8) (2019) 1018–1038.
[54] D.S. Lark, L.R. Reese, T.E. Ryan, M.J. Torres, C.D. Smith, C.T. Lin, et al., Protein kinase a governs oxidative phosphorylation kinetics and oxidant emitting potential at complex I, Front. Physiol. 6 (2015) 332.
[55] X. Chen, N. Baumlin, J. Buck, L.R. Levin, N. Fregien, M. Salathe, A soluble adenylyl cyclase form targets to axonemes and rescues beat regulation in soluble adenylyl cyclase knockout mice, Am. J. Respir. Cell Mol. Biol. 51 (6) (2014) 750–760.
[56] A. Schmid, Z. Sutto, M.C. Nlend, G. Horvath, N. Schmid, J. Buck, et al., Soluble adenylyl cyclase is localized to cilia and contributes to ciliary beat frequency regulation via production of cAMP, J Gen Physiol 130 (1) (2007) 99–109.
[57] J. Buck, M.L. Sinclair, L. Schapal, M.J. Cann, L.R. Levin, Cytosolic adenylyl cyclase defines a unique signaling molecule in mammals, Proc. Natl. Acad. Sci. U. S. A. 96 (1) (1999) 79–84.
[58] B.S. Jaiswal, M. Conti, Identification and functional analysis of splice variants of the germ cell soluble adenylyl cyclase, J. Biol. Chem. 276 (34) (2001) 31698–31708.
[59] J.H. Zippin, Y. Chen, P. Nahirney, M. Kamenetsky, M.S. Wuttke, D.A. Fischman, et al., Compartmentalization of bicarbonate-sensitive adenylyl cyclase in distinct signaling microdomains, FASEB J. 17 (1) (2003) 82–84.
[60] J.H. Zippin, J. Farrell, D. Huron, M. Kamenetsky, K.C. Hess, D.A. Fischman, et al., Bicarbonate-responsive "soluble" adenylyl cyclase defines a nuclear cAMP microdomain, J. Cell Biol. 164 (4) (2004) 527–534.
[61] Q. Feng, Y. Zhang, Y. Li, Z. Liu, J. Zuo, F. Fang, Two domains are critical for the nuclear localization of soluble adenylyl cyclase, Biochimie 88 (3) (2006) 319–328.
[62] M. Zaccolo, T. Pozzan, Discrete microdomains with high concentration of cAMP in stimulated rat neonatal cardiac myocytes, Science 295 (5560) (2002) 1711–1715.
[63] K. Lefkimmiatis, D. Leronni, A.M. Hofer, The inner and outer compartments of mitochondria are sites of distinct cAMP/PKA signaling dynamics, J. Cell Biol. 202 (3) (2013) 453–462.
[64] L. Fazal, M. Laudette, S. Paula-Gomes, S. Pons, C. Conte, F. Tortosa, et al., Multifunctional mitochondrial Epac1 controls myocardial cell death, Circ. Res. 120 (4) (2017) 645–657.
[65] G. Szanda, E. Wisniewski, A. Rajki, A. Spat, Mitochondrial cAMP exerts positive feedback on mitochondrial Ca(2+) uptake via the recruitment of Epac1, J. Cell Sci. 131 (10) (2018).
[66] Z. Wang, D. Liu, A. Varin, V. Nicolas, D. Courilleau, P. Mateo, et al., A cardiac mitochondrial cAMP signaling pathway regulates calcium accumulation, permeability transition and cell death, Cell Death Dis. 7 (2016), e2198.
[67] A.M. Stessin, J.H. Zippin, M. Kamenetsky, K.C. Hess, J. Buck, L.R. Levin, Soluble adenylyl cyclase mediates nerve growth factor-induced activation of Rap1, J. Biol. Chem. 281 (25) (2006) 17253–17258.
[68] J.P. Flacke, H. Flacke, A. Appukuttan, R.J. Palisaar, J. Noldus, B.D. Robinson, et al., Type 10 soluble adenylyl cyclase is overexpressed in prostate carcinoma and controls proliferation of prostate cancer cells, J. Biol. Chem. 288 (5) (2013) 3126–3135.
[69] A. Appukuttan, J.P. Flacke, H. Flacke, A. Posadowsky, H.P. Reusch, Y. Ladilov, Inhibition of soluble adenylyl cyclase increases the radiosensitivity of prostate cancer cells, Biochim. Biophys. Acta. 1842 (12 Pt B) (2014) 2656–2663.
[70] Y. Liao, T. Satoh, X. Gao, T.G. Jin, C.D. Hu, T. Kataoka, RA-GEF-1, a guanine nucleotide exchange factor for Rap1, is activated by translocation induced by association with Rap1*GTP and enhances Rap1-dependent B-Raf activation, J. Biol. Chem. 276 (30) (2001) 28478–28483.
[71] V. Pizon, M. Desjardins, C. Bucci, R.G. Parton, M. Zerial, Association of Rap1a and Rap1b proteins with late endocytic/phagocytic compartments and Rap2a with the Golgi complex, J. Cell Sci. 107 (Pt 6) (1994) 1661–1670.
[72] N. Krahmer, B. Najafi, F. Schueder, F. Quagliarini, M. Steger, S. Seitz, et al., Organellar proteomics and phospho-proteomics reveal subcellular reorganization in diet-induced hepatic steatosis, Dev. Cell 47 (2) (2018) 205–221 (e207).
[73] D.V. Titov, V. Cracan, R.P. Goodman, J. Peng, Z. Grabarek, V.K. Mootha, Complementation of mitochondrial electron transport chain by manipulation of the NAD+/NADH ratio, Science 352 (6282) (2016) 231–235.
[74] M.K. Gaitonde, E. Murray, V.J. Cunningham, Effect of 6-phosphogluconate on phosphoglucose isomerase in rat brain in vitro and in vivo, J. Neurochem. 52 (5) (1989) 1348–1352.
[75] C.W. Parr, Inhibition of phosphoglucose isomerase, Nature 178 (4547) (1956) 1401.
[76] P. Bruch, K.D. Schnackerz, J.M. Chirgwin, E.A. Noltmann, Binding studies on rabbit-muscle phosphoglucose isomerase, Eur. J. Biochem. 36 (2) (1973) 564–568.
[77] K.K. Tsuboi, K. Fukunaga, C.H. Chervenka, Phosphoglucose isomerase from human erythrocyte. Preparation and properties, J. Biol. Chem. 246 (24) (1971) 7586–7594.
[78] M. Salas, E. Vinuela, A. Sols, Spontaneous and enzymatically catalyzed Anomerization of glucose 6-phosphate and Anomeric specificity of related enzymes, J. Biol. Chem. 240 (1965) 561–568.
[79] P. Jiang, W. Du, X. Wang, A. Mancuso, X. Gao, M. Wu, et al., p53 regulates biosynthesis through direct inactivation of glucose-6-phosphate dehydrogenase, Nat. Cell Biol. 13 (3) (2011) 310–316.
[80] A. Benito, I.H. Polat, V. Noe, C.J. Ciudad, S. Marin, M. Cascante, Glucose-6-phosphate dehydrogenase and transketolase modulate breast cancer cell metabolic reprogramming and correlate with poor patient outcome, Oncotarget 8 (63) (2017) 106693–106706.
[81] P. Rodriguez-Rodriguez, E. Fernandez, J.P. Bolanos, Underestimation of the pentose-phosphate pathway in intact primary neurons as revealed by metabolic flux analysis, J. Cereb. Blood Flow Metab. 33 (12) (2013) 1843–1845.
[82] J.C. Street, A.A. Alfieri, J.A. Koutcher, Quantitation of metabolic and radiobiological effects of 6-aminonicotinamide in RIF-1 tumor cells in vitro, Cancer Res. 57 (18) (1997) 3956–3962.
[83] J.C. Street, U. Mahmood, D. Ballon, A.A. Alfieri, J.A. Koutcher, 13C and 31P NMR investigation of effect of 6-aminonicotinamide on metabolism of RIF-1 tumor cells in vitro, J. Biol. Chem. 271 (8) (1996) 4113–4119.
[84] V.P. Sukhatme, B. Chan, Glycolytic cancer cells lacking 6-phosphogluconate dehydrogenase metabolize glucose to induce senescence, FEBS Lett. 586 (16) (2012) 2389–2395.
[85] R.L. Tyson, J. Perron, G.R. Sutherland, 6-Aminonicotinamide inhibition of the pentose phosphate pathway in rat neocortex, Neuroreport 11 (9) (2000) 1845–1848.
[86] F.C. Kauffman, E.C. Johnson, Cerebral energy reserves and glycolysis in neural tissue of 6-aminonicotinamide-treated mice, J. Neurobiol. 5 (5) (1974) 379–392.
[87] N.N. Pavlova, C.B. Thompson, The emerging hallmarks of Cancer metabolism, Cell Metab. 23 (1) (2016) 27–47.
[88] R.J. DeBerardinis, N.S. Chandel, Fundamentals of cancer metabolism, Sci. Adv. 2 (5) (2016), e1600200.

[89] J. Zhang, E. Nuebel, G.Q. Daley, C.M. Koehler, M.A. Teitell, Metabolic regulation in pluripotent stem cells during reprogramming and self-renewal, Cell Stem Cell 11 (5) (2012) 589–595.
[90] B. Kelly, L.A. O'Neill, Metabolic reprogramming in macrophages and dendritic cells in innate immunity, Cell Res. 25 (7) (2015) 771–784.
[91] L. Ramos-Espiritu, A. Diaz, C. Nardin, A.J. Saviola, F. Shaw, T. Plitt, et al., The metabolic/pH sensor soluble adenylyl cyclase is a tumor suppressor protein, Oncotarget 7 (29) (2016) 45597–45607.
[92] J.P. Schwartz, J.V. Passonneau, G.S. Johnson, I. Pastan, The effect of growth conditions on NAD+ and NADH concentrations and the NAD+:NADH ratio in normal and transformed fibroblasts, J. Biol. Chem. 249 (13) (1974) 4138–4143.
[93] Y. Zhao, Q. Hu, F. Cheng, N. Su, A. Wang, Y. Zou, et al., SoNar, a highly responsive NAD+/NADH sensor, allows high-throughput metabolic screening of anti-tumor agents, Cell Metab. 21 (5) (2015) 777–789.
[94] S.C. Lin, D.G. Hardie, AMPK: sensing glucose as well as cellular energy status, Cell Metab. 27 (2) (2018) 299–313.
[95] J.S. Mo, Z. Meng, Y.C. Kim, H.W. Park, C.G. Hansen, S. Kim, et al., Cellular energy stress induces AMPK-mediated regulation of YAP and the hippo pathway, Nat. Cell Biol. 17 (4) (2015) 500–510.
[96] W. Wang, Z.D. Xiao, X. Li, K.E. Aziz, B. Gan, R.L. Johnson, et al., AMPK modulates hippo pathway activity to regulate energy homeostasis, Nat. Cell Biol. 17 (4) (2015) 490–499.
[97] X. Wang, et al., Cholesterol stabilizes TAZ in hepatocytes to promote experimental non-alcoholic steatohepatitis, Cell Metab. 31 (5) (2020) 969–986, https://doi.org/10.1016/j.cmet.2020.03.010.